Giant thermopower of ionic gelatin near room temperature

Giant thermopower of ionic gelatin near room temperature

Cheng-Gong Han[1,3†], Xin Qian[2†], Qikai Li[1,6], Biao Deng[1], Yongbin Zhu[1], Zhijia Han[1], Wenqing Zhang[4], Weichao Wang[5], Shien-Ping Feng[6], Gang Chen[2*], Weishu Liu[1,3*]

[1]Department of Materials Science and Engineering, Southern University of Science and Technology, Shenzhen, Guangdong 518055, China

[2]Dapartment of Mechanical Engineering, Massachusetts Institute of Technology, Cambridge, MA 02139, USA

[3] Shenzhen Engineering Research Center for Novel Electronic Information Materials and Devices, Southern University of Science and Technology, Shenzhen 518055, China

[4]Department of Physics and Shenzhen Institute for Quantum Science & Technology, Southern University of Science and Technology, Shenzhen 518055, China

[5]Department of Electronics and Tianjin Key Laboratory of Photo-Electronic Thin Film Device and Technology, Nankai University, Tianjin 300071, China

[6]Department of Mechanical Engineering, The University of Hong Kong, Pokfulam, Hong Kong 999077, China

†: Equivalent contributions

[*]**Email**: *liuws@sustech.edu.cn*; *gchen2@mit.edu*

Abstract:

Harvesting heat from the environment into electricity has the potential to power Internet-of-Things (IoT) sensors, freeing them from cables or batteries especially for use as wearable devices. We demonstrate a giant positive thermopower of 17.0 mV K^{-1} in a flexible, quasi-solid state, ionic thermoelectric material using synergistic thermodiffusion and thermogalvanic effects. The ionic thermoelectric material is a gelatin matrix modulated with ions providers (KCl, NaCl, and KNO_3) for thermodiffusion effect and redox couple ($Fe(CN)_6^{4-}/Fe(CN)_6^{3-}$) for thermogalvanic effect. A proof-of-concept wearable device consisting of 25 unipolar elements generated over 2 V and a peak power of 5 μW using body heat. This ionic gelatin shows promises for environmental heat-to-electric energy conversion utilizing ions as energy carriers.

Key words: Giant thermopower; Energy harvesting; Gelatin; Thermodiffusion; Thermogalvanic

One Sentence Summary: An ionic gelatin material shows a giant thermopower due to the synergy of thermodiffusion and thermogalvanic effects.

The need to power IoT sensors without using cables or batteries spurs intense research on energy harvesting from environment. One approach is the thermoelectric energy conversion technology, based on the Seebeck effect, using the widely existing waste heat to meet the power demands of IoT sensors from μW to mW (1,2). The conventional electronic-thermoelectric (e-TE) materials usually are narrow-bandgap semiconductors that utilize the electrons or holes as the energy carriers. For a typical thermoelectric material, thermopower (or Seebeck coefficient) is about 100 - 200 $\mu V\ K^{-1}$. As a result, generating a useful voltage of 1 - 5 V in a room temperature environment requires either challenging integration of thousands or even ten thousands of tiny, ~50 μm, thermoelectric elements (3), or a DC-DC voltage booster to increase the voltage of a regular sized device with millimeter legs up to 100 times (4).

An alternative route for direct energy harvesting from low-grade heat was reported in ionic systems, exploring two distinctly different mechanisms. One mechanism is based on redox reactions at two electrodes maintained at two different temperatures. Devices utilizing this mechanism are called thermogalvanic cells (5,6). The other mechanism is ionic thermodiffusion under a temperature gradient without redox reaction, also known as the Soret effect (7,8). Electricity can be generated continuously based on the thermogalvanic mechanism as the redox reactants are rebalanced by ionic diffusion (9). Thermodiffusion cells operate in a capacitive mode (10). After a temperature difference establishes a voltage difference, the charges stored on the electrodes can be discharged to an external load. The temperature gradient is removed for the system to recover, and reapplied for next cycle. Most research is based on either the thermogalvanic cell or the thermodiffusion cell configuration. For the thermogalvanic cells, liquid electrolytes with redox couples such as cobalt(II/III) tris(bipyridyl) (11,12), iron(II/III) (13), iodide/triiodide (14,15), and ferro/ferricyanide ($Fe(CN)_6^{4-}/Fe(CN)_6^{3-}$) (9,16-23) were reported to possess an absolute temperature coefficient of a few mV K^{-1}. For example, one of the highest negative temperature coefficient of -4.2 mV K^{-1} was realized in aqueous system using $Fe(CN)_6^{4-}/Fe(CN)_6^{3-}$ redox couple and chaotropic guanidium salts (22). For the thermodiffusion cell configuration, a thermopower of +11 mV K^{-1} was obtained using NaOH in polyethylene oxide (PEO) solution (10). Liquid cells, however, have a drawback for use in wearable devices due to the challenges of encapsulation (24-26). Quasi-solid state electrolytes have gained attentions as an alternative (27-29). A temperature coefficient of -1.09 and -1.21 mV K^{-1} was observed when employing $Fe(CN)_6^{4-}/Fe(CN)_6^{3-}$ as redox couple in the poly-sodium acrylate

and polyvinyl alcohol matrix, respectively (27,28), lower than that of the redox couple in liquid solutions. Interestingly, high thermodiffusive thermopower is observed in quasi-solid state polymer gel composite of PVDF and PEG with ionic liquid as charge carriers, and the thermopower is tunable from -4 mV K^{-1} to 14 mV K^{-1} by tailoring the composition (29). Furthermore, a thermopower as high as +24 mV K^{-1} was reported by using the high ionic selectivity of the NaOH-PEO aqueous solution in the confined nanocelluosic channels, such that Na^+ is the major mobile ions (30). However, whether the thermodiffusion effect and thermogalvanic effect synergistically work together to boost the final thermopower in a single ionic thermoelectric (i-TE) system, remains an open question because of their fundamentally different physical pictures.

We combined thermogalvanic and thermodiffusion effects to achieve high thermopower. Before moving on, however, it is necessary to clarify our terminologies as the literature has created some confusion. Similar to conventional e-TE materials, the thermodiffusive thermopower (or Seebeck coefficient) of ions is defined as $S_{td} = -\frac{V(T_H)-V(T_C)}{T_H-T_C}$, where $V(T_H)$ and $V(T_C)$ correspond to the voltage of the hot electrode at temperature T_H and the cold electrode at temperature T_C, respectvely. We clarify later that the sign of S_{td} is determined by the type of charge with higher thermal mobility in a solution, and hence is a transport property. In electrochemistry, the temperature dependence of the standard electrode potential for a reduction reaction (E^0) at the isothermal condition is referred as "temperature coefficient", as $\alpha_R = dE^0/dT$ (31,32). α_R is a thermodynamic property. For a redox reaction $O + ne \leftrightharpoons R$, where the oxidized species O is converted into the reduced species R with n mole of electrons transferred per unit mole of reaction, the temperature coefficient is $\alpha_R = \frac{s_R - s_O}{nF}$, where s_O and s_R are partial molar entropies of the species O and R, respectively, and F is the Faraday constant. In a thermogalvanic cell under a temperature gradient, the redox reaction contribution to the measured voltage is $V(T_H) - V(T_C) = \alpha_R (T_H - T_C)$, which means that the sign of α_R is opposite to the sign convention of the Seebeck coefficient (33). In addition to the redox contributions, the thermodiffusion of redox species under a temperature gradient also contributes to the total voltage, which is usually negligible (~ 10 μV K^{-1}) in aqeuous solutions (33). We report a giant thermopower of 17.0 mV K^{-1} in a quasi-solid state i-TE material by combining the thermodiffusion effect of KCl and temperature coefficient of $Fe(CN)_6^{4-}/Fe(CN)_6^{3-}$ redox couple. The general strategy is to utilize a negative temperature coefficient (i.e., $\alpha_R < 0$) and a p-type thermodiffusive thermopower ($S_{td} > 0$) to generate a high differential thermal voltage S_i. Using such materials, a high output voltage of 2.2 V is achieved using body heat in a wearable and flexible i-TE device with only 25 unipolar

elements in series working in a quasi-continuous mode. The proof-of-concept device demonstrates promising application of ionic gelatin in powering wearable IoT applications.

Giant thermopower of i-TE materials

We denote the as-fabricated i-TE materials as Gelatin-*x* MX-*m*/*n* $FeCN^{4-/3-}$ (MX = KCl, NaCl, KNO_3), where *x* and *m*/*n* are the molar concentration of MX and $K_4Fe(CN)_6/K_3Fe(CN)_6$, respectively, in which the $Fe(CN)_6^{4-}/Fe(CN)_6^{3-}$ serves as the redox couple (hereafter, abbreviated as $FeCN^{4-/3-}$) and ion provider MX further boosts the thermodiffusive thermopower. We chose organic gelatin for the matrix due to its abundance, low cost, high biocompatibility, and mechanical flexibility. We found that thermodiffusion of ionic species under a temperature gradient, together with the thermogalvanic effect of redox couple $FeCN^{4-/3-}$, contributes to the high thermopower of i-TE materials of Gelatin-*x* KCl-*m*/*n* $FeCN^{4-/3-}$. We observed an improved thermopower from 4.8 mV K^{-1} to 12.7 mV K^{-1} by increasing the concentration of KCl from *x* = 0 M to 0.8 M in the as-fabricated Gelatin-*x* KCl-0.42/0.25M $FeCN^{4-/3-}$ (Fig. 1A, Fig. S1). We achieved a further improved thermopower from 12.7 mV K^{-1} to 17.0 mV K^{-1} by tailoring the volume ratio of water to gelatin (Fig. 1A). This value is much higher than other reported gel-based i-TE materials by using either thermodiffusion effect or thermogalvanic effect (Fig. 1B, Table S1).

The thermodiffusion of KCl in gelatin showed a p-type thermopower. We then employed the $FeCN^{4-/3-}$ redox couple, which has a negative temperature coefficient, to achieve a synergistic effect. Because α_R is related to the entropy change of reduction reaction, the negative temperature coefficient $\alpha_R = \frac{S_{FeCN^{4-}} - S_{FeCN^{3-}}}{F} < 0$ indicates that $FeCN^{4-}$ has lower solvation entropy than $FeCN^{3-}$, which is consistent with the solvation shell being more tightly packed around $FeCN^{4-}$ due to its higher valence charge (35). At the hot electrode, the oxidation reaction $FeCN^{4-} \rightarrow e + FeCN^{3-}$ is thermodynamically favorable, which injects electrons into the hot electrode and increases its electrochemical potential (i.e. lower voltage) and generates a thermopower (33) that is consistent with the thermodiffusion contributions of KCl. At the cold side, the reduction reaction $FeCN^{3-} + e \rightarrow FeCN^{4-}$ is thermodynamically favored with electrons attracted from the electrode, resulting in a decreased electrochemical potential (higher voltage). The redox couple therefore synergistically worked together to achieve the high p-type thermopower in the as-fabricated i-TE materials of Gelatin-*x* KCl-*m*/*n* $FeCN^{4-/3-}$.

Optimization of thermopower

The optimization of the as-fabricated i-TE materials of Gelatin-*x* MX-*m*/*n* $FeCN^{4-/3-}$ involved tuning of the concentration of the ion providers (MX = KCl, KNO_3 and NaCl), the redox couple ($FeCN^{4-/3-}$), and the volume ratio of water to gelatin. We obtained a thermopower of 1.4 mV K^{-1} from $V(T_C)$ - $V(T_H)$ and T_H - T_C measurements (Fig. S1) for the $FeCN^{4-/3-}$ redox couple in aqueous electrolyte with Cu foils as the symmetric electrodes (Cu | aqueous $FeCN^{4-/3-}$ | Cu). Our measurements were in good agreement with the previously reported value (1.4 mV K^{-1}) (9). We observed a leap in thermopower from 1.4 mV K^{-1} to 4.8 mV K^{-1} in Gelatin-$FeCN^{4-/3-}$ (*m*/*n* = 0.42/0.25 M) compared with the pristine $FeCN^{4-/3-}$ solution (Fig. S1). The pure gelatin had a reference thermopower of 1.3 mV K^{-1} due to the thermodiffusion of H^+ from the ionization of carboxyl groups –COOH (36), while the Gelatin-*m* $FeCN^{4-}$ (*m* = 0.42 M) and Gelatin-*n* $FeCN^{3-}$ (*n* = 0.25 M) had a thermopower of 1.2 mV K^{-1} and 1.0 mV K^{-1} (Fig. S2 A), respectively.

We investigated the thermodiffusion effect of ion providers by comparing three series of gelatin-based i-TE materials, i.e. Gelatin-*x* KCl, Gelatin-*x* KNO_3 and Gelatin-*x* NaCl with *x* = 0, 0.1, 0.3, 0.5, 0.8 and 1 M, respectively (Fig. 1C, Fig. S3). Gelatin-*x* KCl had an increased thermopower from 4.3 mV K^{-1} to a peak value of 6.7 mV K^{-1} as the concentration of KCl increased from *x* = 0.3 M to 0.8 M, and then a decline when further increasing the concentration of KCl. The Gelatin-*x* NaCl also had a similar peak thermopower of ~ 6.7 mV K^{-1} but at the concentration of *x* = 0.3 M. The Gelatin-*x* KNO_3 had a lower peak thermopower around 3 - 4 mV K^{-1} in the range of *x* = 0.5 - 0.8 M.

Theoretically, the contribution to the thermopower of mobile cations and anions in i-TE materials could be analogous to the multi-bands transport in e-TE materials. Temperature gradient drives both cations and anions to migrate across the device from the hot side to the cold side, resulting in a net charge accumulation and an internal electric field that generated voltage. We derived the total thermodiffusive thermopower of a symmetrical electrolyte, such as Gelatin-*x* KCl, based on the Onsager transport theory as following (33):

$$S_{td} = \frac{D_+\hat{S}_+ - D_-\hat{S}_-}{e(D_+ + D_-)} \qquad \text{(eq. 1)}$$

where the subscript $i = \pm$ denotes the ion species, *e* is the elementary charge, D_i and $\hat{S}_i$ are the mass diffusion coefficient and the Eastman entropy of transfer, respectively. $\hat{S}_i$ is essentially the temperature dependence of the free energy d*G*/d*T*, which is related to the interaction between solutes and the surrounding media (37). Cations and anions in i-TE materials are equal so that the ionic thermodiffusion is ambipolar, a difference from e-TE materials. Analogous to Einstein relation for diffusion driven by concentration gradient, a thermal mobility can also be defined as $D_i\hat{S}_i/k_BT$

(33). The positive thermopower suggested that the thermal mobility ($D_+\hat{S}_+/k_BT$) of cation K^+ was larger than that ($D_i\hat{S}_i/k_BT$) of anion Cl^-. The ionic interactions induced by negative-charged gelatin network could generate a larger Eastman entropy of transfer $\hat{S}_+$, which might be responsible for the large p-type thermodiffusive thermopower. Alternatively, the complicated relation between the diffusion coefficient and the concentration in the matrix with a charged polymer network may also be responsible. Experiments (38) and computational analysis (39,40) showed that in a negatively charged polymer network, the cations showed a higher diffusion coefficient. A small fraction of cations tends to "condensate" along a negatively charged polymer chains. This "counterion condensation" was proposed by G. S. Manning (41). These immobilized K^+ condensed near the polymer could further impose frictional drags on Cl^-, which reduced the mobility of Cl^-. However, the rest of K^+ not condensed around the polymer backbones remains more mobile compared with the Cl^- that was dragged by the condensed immobile K^+. We observed that the thermopower is concentration dependent. As the concentration increases, the fraction of mobile cations increases as compared with the condensed cations (39). Further increasing concentration could decrease the Debye length of the electrical double layer and induced a screening effect of the ionic coupling between the ions and gelatin, and the thermal mobility of ions tends to converge to pure KCl solution which has negligibly small thermopower measured to be ~ 40 μV K^{-1} (34). This tradeoff could explain the optimal concentration for maximum thermopower in Gelatin-*x* KCl and Gelatin-*x* KNO_3. The lower thermopower of Gelatin-*x* KNO_3 than Gelatin-*x* KCl can also be attributed to the smaller difference between the thermal mobility of K^+ and NO_3^-. NO_3^- is a stronger water-structure-breaker as compared with Cl^-, resulting in a higher mass diffusion coefficient D_- (42), which is consistent with the ionic conductivity measurement (Fig. S4). Thus, the NO_3^- cancels more thermopower than Cl^- in the as-fabricated gelatin-based i-TE materials. Moreover, we found that the pH values affect the thermopower of i-TE material, i.e. Gelatin-*x* KCl (*x* = 0.8 M) (Fig. 1D, Fig. S5 A-B), because of the ionization of gelatin functional groups (-COOH), which could affect the ion-gelatin interaction and effectively change the Eastman entropy of transfer of ions. We observed an optimized thermopower of 6.7 mV K^{-1} at pH = 7.0. Additionally, we also investigated the Gelatin-*x* K_2SO_4 (*x* = 0.25, 0.40 and 0.50 M) with divalent anions (Fig. S5 C). Among the investigated concentrations, the Gelatin-*x* K_2SO_4 (*x* = 0.40 M) showed the highest thermopower 4.9 mV K^{-1}, which is much less than that 6.7 mV K^{-1} of Gelatin-*x* KCl (*x* = 0.8 M).

Adding $FeCN^{4-/3-}$ into the Gelatin-*x* KCl system makes the thermopower sensitive to the concentration of $FeCN^{4-/3-}$ redox couple. The thermopower varied from 6.7 mV K^{-1} to 8.3, 10.4, 12.7 and 7.7 mV K^{-1}, as *x* = 0.8 M while *m*/*n*

changed from 0/0 M to 0.08/0.05, 0.25/0.15, 0.42/0.25 and 0.50/0.30 M, respectively (Fig. 1E, Fig. S2 B). We repetitively observed the highest thermopower of 12.7 mV K^{-1} in the as-fabricated i-TE material of Gelatin-0.8 KCl-0.42/0.25M $FeCN^{4-/3-}$ (Fig. S6). We measured lower thermopower of Gelatin-0.8 M KCl-*m*/*n* $FeCN^{4-/3-}$ with *m*/*n* = 0.25/0.25 M (11.0 mV K^{-1}) and 0.42/0.42 M (7.3 mV K^{-1}) than *m*/*n* = 0.42/0.25 M (Fig. S2 C). We attribute the high thermopower to the synergy of the thermogalvanic effect of redox couple $FeCN^{4-/3-}$ and the thermodiffusion effect of the mobile ions. Additionally, the thermal conductivity of the i-TE material Gelatin-0.8M KCl-0.42/0.25M $FeCN^{4-/3-}$ is low (0.15 W m^{-1} K^{-1} at 293 K), allowing it to maintain a temperature difference for power generation (Fig. S7) (33). We observed excellent reversibility of the redox reaction evidenced by the overlapped peaks scanned for three cycles in CV curves (Fig. S8). We observed the anodic and cathodic peaks from 0.05 V to 0.28 V and -0.05 V to -0.28 V (vs. Pt), respectively, in the CV curves of the Gelatin-0.8 M KCl-*m*/*n* $FeCN^{4-/3-}$ (Fig. S9 A). We found increasing redox peak potential (E_p) and current density with increasing *m*/*n* values (Fig. S9 B). Additionally, the oxidized species ($FeCN^{3-}$) generated at the hot side and the reduced species ($FeCN^{4-}$) generated at the cold side migrated to the other electrode under a concentration gradient, making continuous current output possible (9,43).

The water/gelatin volume ratio (r_v) also boosted the thermopower of the as-fabricated Gelatin-0.8M KCl-0.42/0.25M $FeCN^{4-/3-}$ system. The water in the gelatin matrix provides the diffusion channel for ions in the quasi-solid state i-TE material, impacting the thermopower (Fig. 1F, Fig. S10). We varied r_v values and observed a continuous increase from 12.7 to 17.0 mV K^{-1} as r_v increased from 2.0 to 3.0. Increasing r_v further to 3.3 decreased thermopower to 14.1 mV K^{-1} (Fig. 1F). Higher r_v also reduced the fracture strain and stretchability. We fixed r_v = 2.0 for device demonstration.

Mechanism of synergistic effect

This section explains the synergy between the thermodiffusion and thermogalvanic effects (Fig. 2A-C). The thermodiffusion of KCl accumulated positive net charges near the cold electrode, generating an electric field pointing from the cold electrode to the hot electrode (Fig. 2A). This generated a thermodiffusive voltage $\Delta V_{td} = -\frac{\tilde{\mu}_{TH}-\tilde{\mu}_{TC}}{e} = V(T_H) - V(T_C) < 0$. The higher solvation entropy generates more $FeCN^{3-}$ than $FeCN^{4-}$ at higher T (35) through oxidation. This transfers electrons to the hot electrode increases the chemical potential ($\tilde{\mu}_{TH}$). $FeCN^{4-}$ generation was promoted and extracted electrons from the cold electrode. The T gradient drives thermodiffusion and balances the redox reaction. Consequently, the thermogalvanic effect shifted the $\tilde{\mu}$ of both electrodes in the same direction as the

thermodiffusion effect. The thermogalvanic voltage we measured was the difference in standard electrode potential $\Delta E^0 = -\frac{\tilde{\mu}_{TH}-\tilde{\mu}_{TC}}{e} < 0$, which has the same sign as the thermodiffusive voltage. The $FeCN^{4-/3-}$ also participated in thermodiffusion and contributed to the final thermopower.

From the Onsager transport formulation, we see how a large positive thermopower comes from the coupling of the thermodiffusion and thermogalvanic effects (33). We derived that the total thermopower S_i could be written as a summation:

$$S_i = -\alpha_R + S_{td}(K^+ - FeCN^{4-/3-}) + S_{td}(KCl) + S_{td}(gelatin) \quad \text{(eq. 2)}$$

where $-\alpha_R$ is the contribution to thermopower due to the redox reaction $Fe(CN)_6^{3-}$ + e ⇋ $Fe(CN)_6^{4-}$, S_{td} is the thermopower due to the thermodiffusion of mobile ions, and S_{td} (gelatin) is the intrinsic thermopower of the gelatin. We used an isothermal three-electrode system (Fig. 2D) to effectively eliminate the T gradient and determine the temperature coefficient (33). The contribution from the redox couple is finally determined as $-\alpha_R$ = 2.27 mV K^{-1} (Fig 2E, Fig. S11) by compensating the temperature coefficient of SCE (33). Fig. 2F shows the schematic illustration of partial contribution thermopower in a complex system containing K^+, Cl^-, $FeCN^{4-/3-}$ and water as well as gelatin molecule structure. Relative contribution to the total thermopower in Gelatin-0.8M KCl-0.42/0.25M $FeCN^{4-/3-}$ (, r_v = 2.0) is determined as (Fig. 2G): 10.2% contribution of Gelatin, 17.9% of redox entropy of $FeCN^{4-/3-}$, 9.7% contribution of thermodiffusion of $K_3Fe(CN)_6$ and $K_4Fe(CN)_6$, and 62.2% contribution of thermodiffusion effect of KCl (33)

We conducted experiments by switching the direction of the temperature differences between two electrodes, and observed a hysteresis showing the dynamical response of the device to the transient temperature field (Fig. S12, S13) (33).

Working modes of an i-TE cell

A thermodiffusion effect based i-TE cell is essentially capacitive (10,30) because the discharge current is non-faradaic and no electrons transport across the electrode electrolyte interfaces, while a thermogalvanic cell works in a continuous manner with redox couples reacting in opposite directions on the hot and cold electrodes with ionic diffusion supplying the reactants to electrode surfaces ensuring continuous operation (9). We demonstrate a quasi-continuous working mode by using the i-TE material of Gelatin-0.8M KCl-0.42/0.25M $FeCN^{4-/3-}$(r_v = 2.0). We assembled the i-TE cell in a laminar structure of Cu | Au | i-TE | Au | Cu (15 × 15 × 1.8 mm). We maintained the cold

side at 293 K with the hot side at 301.5 K (ΔT = 8.5 K). The as-fabricated i-TE cell was charged in ~ 55 min to reach a high (near-saturation) voltage. We then stepped it into the quasi-continuous working mode. The cell discharged to 0 V in 10 s in short-circuit, and then recovered back to the high voltage in 3 min in open-circuit under the same applied temperature difference. In the discharge process, the electrons flow from the hot side to cold side through the external circuit, resulting in a decreased internal electrostatic field and hence the cell voltage. The discharging current is also a synergistic result of redox couples and ion providers, contributed partially by faradaic process due to the redox couple $FeCN^{4-/3-}$ and the capacitive desorption of K^+ and Cl^-. Once the external circuit is disconnected, the diffusion of the redox couple re-supply the consumed species to the electrode, and concentration profile of ion providers re-establishes, such that the cell voltage recovers allowing for the next discharge cycle (Fig. S14). We completed 100 of these charge-discharge cycles (Fig. 3A) over a time span of 5 hours. The corresponding power curve of the 5th cycle displayed parabolic behavior with the maximum at 8 μW (Fig. 3B). We expect that such quasi-continuous operation can last much longer until the electrodes are fully polarized (33). Output power decreased as quasi-continuous cycle number increases (Fig 3C, inset), which is probably due to the polarization of the electrodes. To solve this issue, we reactivated the i-TE cell by removing the temperature difference and totally cooling down the cell while short-circuiting the electrodes. The reactivated cell recovered the voltage and current (Fig. S15). The concentrations of all the ionic species redistributed and electrodes were depolarized after this process (33). We reproducibly achieved high thermally charged voltage over several consecutive days (Fig. S16). This demonstrates that the cell can be repetitively used rather than as a one-time energy source. We reduced the thermal charge time from 3 min to roughly 20 seconds by increasing the layer number of the i-TE cell from a single layer to 3-layers (Cu | i-TE | Cu | i-TE | Cu | i-TE | Cu, 15 × 15 × 1.8 mm). The internal electrode shortened the time for ions to diffuse across the shortened distance, and hence shortened the thermal charging process (Fig. S17).

We coated the Cu foils (10 μm thickness) with Au (40 nm) as electrode corrosion is a performance concern. We found a comparable thermopower (Fig. S18). However, the total energy density of initial 50 cycles was much higher (7.4 J m^{-2}) than for Cu-foil electrodes (1.5 J m^{-2}) (Fig. S19). The Au (40 nm) coated Cu-foil electrode has enlarged surface area (Fig. S20) (21,44). We also measured a slightly (8%) higher thermopower using a Pt electrode compared to the Cu foil electrode (Fig. S21). Electrode optimization may boost the output power density of gelatin-based i-TE cell. We calculated the specific pulsed power density, $P_{max}/(\Delta T)^2 = V_{oc}I_{sc}/(2\Delta T)^2$, where V_{oc} and I_{sc} are the open-circuit

voltage and short-circuit current respectively. We measured the maximum output power density to be 0.66 mW m^{-2} K^{-2}, which is one or two orders higher than previously reported gel-based i-TE cell (Fig. 3C, Table S2).

We show the as-fabricated i-TE cell with Au coated copper electrodes in continuous working mode. We initially thermal-charged the cell at ΔT ~ 8 K to reach a near-saturated voltage and then electrically discharged at the same temperature difference ΔT with a constant external resistance of 5000 Ω (Fig. 3D). The output voltage and output power (Fig. 3E) initially decay rapidly but saturate to a constant value with the external resistor, reaching steady-state thermogalvanic operation mode. We calculated the energy density (Fig. 3F) for a range of external resistance, which has parabolic behavior and saturates at 12.8 J m^{-2}. This value is higher than the continuous working mode (Fig. 3C).

Proof-of-concept wearable i-TE device

An ionic liquid in polymer gel i-TE cell based on thermodiffusion was demonstrated by D. Zhao *et al*. and achieved a device thermopower of 0.33 V K^{-1}. This device combined 18 pairs of n- and p-type elements (29). Using 25 p-type unipolar elements allows us to reach comparable device thermopower. Our i-TE materials are highly flexible and suitable for wearable electronics applications (Fig. S22). After bending the Gelatin-*x* KCl-*m*/*n* $FeCN^{4-/3-}$ 5000 times, it possessed similar values of the voltage and output power density (Fig. S23). The addition of KCl and $FeCN^{4-/3-}$ could potentially improve the stretchability, which we strained to 200% as compared with 140% strain for the pure Gelatin (Fig. S24). The as-fabricated i-TE materials of Gelatin-0.8M KCl-0.42/0.25M $FeCN^{4-/3-}$ (r_v = 2.0) remained intact after stretching from 3 cm to 7.2 cm and recovered after release (Fig. 4A).

The giant thermopower of the as-fabricated ionic gelatin i-TE materials (Gelatin-*x* KCl-*m*/*n* $FeCN^{4-/3-}$) provides a promising solution for the voltage need of IoT sensors near room temperature environment. We constructed a flexible and wearable i-TE device assembled by serially connecting 25 i-TE elements using copper-only electrodes (Fig. 4B). This device can be worn at the back of hand (inset in Fig. 4B). We obtained a voltage of 2.2 V in a cold environment (ΔT of ~10 K). The voltage generated by our device is enough to drive many sensors without additional DC-DC voltage boosters, i.e. humidity sensors (1.6 - 3.6 V), pressure sensors (1.5 - 3.6 V), and gas sensors for monitoring indoor air quality (1.8 - 3.6 V). We measured current-voltage-output power (*I*-*V*-*P*) curves of our 25 elements assembled i-TE device (Fig. 4C). We obtained a pulsed output power of 5.0 μW and a close-circuit current of 8.5 μA in 10 s discharge process, corresponding to the electricity energy of 3.5×10^{-5} J after a single thermal charge. This harvested energy is enough for powering many commercial sensors, i.e. 0.7×10^{-6} J of the digital temperature sensor

(Si705x, from Silicon LABS, operating voltage 1.9 - 3.6 V, 195 nA average current at 1 Hz sample rate), and 1.1 × 10^{-6} J of the low-power humidity sensor (HDC2010, from Texas Instruments, operating voltage 1.6 - 3.6 V, 0.3 μA average current at 1 Hz sample rate). We compared the output voltage and power of our i-TE wearable device with other reported i-TE and e-TE devices that used human body heat (Fig. 4D). Our as-fabricated i-TE wearable device was 2 - 3 times some previously reported i-TE devices (28,45) and 2 orders of magnitude higher than e-TE devices (46-48).

Summary

We demonstrated a giant thermoelectric effect in ionic gelatin based i-TE materials of Gelatin-*x* KCl-*m*/*n* $FeCN^{4-/3-}$, which synergistically combines the thermogalvanic effect of redox couple ($FeCN^{4-/3-}$) and the thermodiffusion effect of ions providers. High positive thermopower of 12.7 ~ 17.0 mV K^{-1} is achieved by comprehensively optimizing the concentration of KCl (*x* = 0.8 M) and $FeCN^{4-/3-}$ (*m*/*n* = 0.42/0.25 M) and water ratio. A proof-of-concept flexible i-TE wearable device with 25 p-type elements shows a high voltage up to 2.2 V, and a pulsed output power of 5.0 μW with total output energy of 3.5 × 10^{-5} J are extracted in a single discharge process by utilizing the real heat of the human body with Δ*T* ~10 K, enough to power many IoT sensors. The generated voltage is 2-3 times higher than the previous reported i-TE devices. The as-fabricated i-TE cell can work in a quasi-continuous thermal-charge/electrical-discharge mode for a long-time usage, but can also work in continuous mode delivering a maximum energy density of 12.8 J m^{-2}. This work provides a promising approach to realize cable-free or battery-free energy supplies for IoT sensors, demonstrating the promise of utilizing ions as the energy carriers in the thermoelectric energy conversion.

References and notes

1. J. He, T. M. Tritt, *Science* **357**, 1369 (2017).

2. M. Haras, T. Skotnicki, *Nano Energy* **54**, 461-476 (2018).

3. E. Mu et al., *Nano Energy* **55**, 494-500 (2019).

4. B. Iezzi, K. Ankireddy, J. Twiddy, M. D. Losego, J. S. Jur, *Appl. Energy* **208**, 758-765 (2017).

5. R. Zito, *AIAA J.* **1**, 2133-2138 (1963).

6. T. I. Quickenden, Y. Mua, *J. Electrochem. Soc.* **142**, 3985-3994 (1995).

7. E. D. Eastman, *J. Am. Chem. Soc*. **50**, 283-291 (1928).

8. H. J. V. Tyrrell, D. A. Taylor, C. M. Williams, *Nature* **177**, 668-669 (1956).

9. R. Hu et al., *Nano Lett.* **10**, 838-846 (2010).

10. D. Zhao et al., *Energy Environ. Sci.* **9**, 1450-1457 (2016).

11. T. J. Abraham, D. R. MacFarlane, J. M. Pringle, *Energy Environ. Sci.* ***6***, 2639-2645 (2013).

12. M. A. Lazar, D. Al-Masri, D. R. MacFarlane, J. M. Pringle, *Phys. Chem. Chem. Phys.* **18**, 1404-1410 (2016).

13. M. A. Buckingham, F. Marken, L. Aldous, *Sustain. Energy Fuels* **2**, 2717-2726 (2018).

14. T. J. Abraham, D. R. MacFarlane, J. M. Pringle, *Chem. Commun.* **47**, 6260-6262 (2011).

15. T. J. Abraham et al., *Electrochim. Acta* **113**, 87-93 (2013).

16. T. J. Kang et al., *Adv. Funct. Mater.* **22**, 477-489 (2012).

17. M. S. Romano et al., *Adv. Mater.* **25**, 6602-6606 (2013).

18. Y. Yang et al., *Proc. Natl. Acad. Sci. U.S.A.* **111**, 17011-17016 (2014).

19. H. Im et al., *Nat. Commun.* **7**, 10600 (2016).

20. T. Kim et al., *Nano Energy* **31**, 160-167 (2017).

21. L. Zhang et al., *Adv. Mater.* **29**, 1605652 (2017).

22. J. Duan et al., *Nat. Commun.* **9**, 5146 (2018).

23. J. H. Kim et al., *Sci. Rep.* 9, 8706 (2019).

24. Y. V. Kuzminskii, V. A. Zasukha, G. Y. Kuzminskaya, *J. Power Sources* **52**, 231-242 (1994).

25. S. L. Kim, H. T. Lin, C. Yu, *Adv. Energy Mater.* **6**, 1600546 (2016).

26. H. Ma et al., *ACS Energy Lett.* 4, 1810-1815 (2019).

27. A. Kundu, T. S. Fisher, *Electrochim. Acta* **281**, 357-369 (2018).

28. P. Yang et al., *Angew. Chem. Int. Edit.* **55**, 12050-12053 (2016).

29. D. Zhao et al., *Nat. Commun.* **10**, 1093 (2019).

30. T. Li et al., *Nat. Mater.* **18**, 608-613 (2019).

31. A. J. deBethune, T. S. Licht, N. Swendeman, *J. Electrochem. Soc*. **106**, 616-625 (1959).

32. S. C. Bratsch, *J. Phys. Chem. Ref. Data* **18**, 1-21 (1989).

33. Materials and Methods are available as Supplementary Materials on Science Online 34. J. N. Agar, C. Y. Mou, J. L. Lin, *J. Phys. Chem*. **93**, 2079-2082 (1989).

35. B. Huang et al., *Phys. Chem. Chem. Phys*. **20**, 15680-15686 (2018).

36. C. M. Ofner III, H. Schott, *J. Pharm. Sci.***74**, 1317-1321 (1985).

37. S. Duhr, D. Braun, *Proc. Natl. Acad. Sci. U.S.A.* **103**, 19678-19682 (2006).

38. J. Kamcev, D. R. Paul, G. S. Manning, B. D. Freeman, *Marcromolecules* **51**, 5519-5529 (2018).

39. D. Aryal, V. Ganesan, *ACS Marcro Lett.* **7**, 739-744 (2018).

40. D. Aryal, V. Ganesan, *J. Chem. Phys.* **149**, 224902 (2018).

41. G. S. Mannining, *J. Phys. Chem.* **88**, 6654-6661 (1984).

42. D. J. Tobias et al., *Science* **319**, 1197 (2008).

43. A. Al-zubaidi, X. Ji, J. Yu, *Sustain. Energy Fuels* **1**, 1457-1474 (2017).

44. H. A. H. Alzahrania, M. A. Buckingham, F. Marken, L. Aldous, *Electrochem. Commun*. **102**, 41-45 (2019).

45. J. Duan et al., *Nano Energy* **57**, 473-479 (2019).

46. S. J. Kim, J. H. We, B. J. Cho, *Energy Environ. Sci.* **7**, 1959-1965 (2014).

47. J. Y. Oh et al., *Energy Environ. Sci.* **9**, 1696-1705 (2016).

48. C. S. Kim et al., *Appl. Energy* **214**, 131-138 (2018).

Acknowledgements

We would like to thank reviewers whose comments have helped us to improve the manuscript significantly, including identifying a sign error in the original manuscript. **Funding:** This work is supported in part by the Centers for Mechanical Engineering Research and Education at MIT and SUSTech (WSL and GC). WSL would like to thank the support of Pearl River Talents Recruitment Program No. 2016ZT06G587 and the Tencent Foundation through the XPLORER PRIZE. WQZ acknowledges the support from the Guangdong Innovation Research Team Project (No. 2017ZT07C062), Guangdong Provincial Key-Lab program (No. 2019B030301001), Shenzhen Municipal Key-Lab program (ZDSYS20190902092905285), and the Shenzhen Pengcheng-Scholarship Program. WCW would like to thank the National key research and development program (Grant No. 2016YFB0901600), Tianjin City Distinguish Young Scholar Fund, National Natural Science Foundation of China (21573117 and 11674289). **Author contributions:** C.-G. Han and W.S. Liu designed the experiment, C.-G. Han, Q.K. Li, B. Deng, Y.B. Zhu and Z.J. Han conducted the experiment. X. Qian and G. Chen carried out the theoretical deviation. C.-G. Han, X. Qian, G. Chen and W.S. Liu completed the writing of the manuscript, W.C. Wang and S.-P. Feng, W.Q. Zhang and G. Chen contributed to the interpretation of the results and revision of the manuscript. All authors discussed the results and participated in revising the

manuscript. **Competing interests:** None declared. **Data and materials availability:** All data are available in the manuscript and supplementary materials.

Figures captions

Fig. 1. Giant thermopower of i-TE materials. (**A**) Comparison of the thermopower among the as-fabricated ionic thermoelectric (i-TE) materials of Gelatin-*x* KCl-*m*/*n* $FeCN^{4-/3-}$ in this work as Gelatin (*x* = 0 M, *m*/*n* = 0 M), Gelatin-$FeCN^{4-/3-}$ (*x* = 0 M, *m*/*n* = 0.42/0.25 M), Gelatin-KCl (*x* = 0.8 M, *m*/*n* = 0 M) and Gelatin-KCl-$FeCN^{4-/3-}$ (*x* = 0.8 M, *m*/*n* = 0.42/0.25 M, volume ratio of water to gelatin r_v = 2.0 and 3.0). (**B**) Absolute thermopower of i-TE materials containing the thermodiffusion effect or the thermogalvanic effect (Table S1). (**C**) Thermopower of i-TE materials of Gelatin-*x* KCl, Gelatin-*x* KNO_3 and Gelatin-*x* NaCl with varying concentration of KCl, KNO_3 and NaCl. (**D**) Thermopower of i-TE materials of Gelatin-*x* KCl, with varying pH values that were tuned by HCl and KOH, respectively. (**E**) Thermopower of i-TE materials of Gelatin-*x* KCl-*m*/*n* $FeCN^{4-/3-}$ with the fixed *x* = 0.8 M. (**F**) Thermopower with the dependence of volume ratio of water to gelatin for Gelatin-0.8M KCl-0.42/0.25M $FeCN^{4-/3-}$. r_v = 2.0 was kept in Fig. (C-E).

Fig. 2. Mechanism of the synergistic effect. Electrochemical potential ($\tilde{\mu}$) of charge carries diagrams and the corresponding voltage (*V*) distribution of i-TE material of Gelatin-*x* KCl-*m*/*n* $FeCN^{4-/3-}$ as (**A**) Gelatin-KCl (*x* = 0.8 M, *m*/*n* = 0 M), *E* represents the built-in electric field, (**B**) Gelatin-$FeCN^{4-/3-}$ (*x* = 0 M, *m*/*n* = 0.42/0.25 M), (**C**) Gelatin-0.8M KCl-0.42/0.25M $FeCN^{4-/3-}$. (**D**) Isothermal system of Gelatin-$FeCN^{4-/3-}$ for measuring the entropy of $FeCN^{4-/3-}$. The work electrode (WE) was platinum, while saturated calomel electrode (SCE) was used as reference electrode (RE) and counter electrode (CE). (**E**) Thermopower due to redox entropy change of $FeCN^{4-/3-}$ ($-\alpha_R$) measured from (D) and total value (S_i). (**F**) Schematic figure of the diffusion, redox reaction, interaction of the ions in the as-fabricated i-TE materials of Gelatin-*x* KCl-*m*/*n* $FeCN^{4-/3-}$ under the temperature gradient. (**G**) Fractional contribution to thermopower of i-TE material Gelatin-*x* KCl-*m*/*n* $FeCN^{4-/3-}$.

Fig. 3. Working mode of an i-TE cell. (**A**) Quasi-continuous thermal-charge/electrical-discharge process for an i-TE cell measured for 100 cycles (Cu | Au | i-TE | Au | Cu, 15 × 15 × 1.8 mm, Au (40 nm) coated rough Cu foils). (**B**)

Power (line, −), voltage (dash line, --) and output current (dash dot line, -·-) curves of discharge process at the 5th cycle in Fig. A. (**C**) Corresponding total energy density of initial 50 cycles for i-TE cell with rough Cu | Au (40 nm) and smooth Cu as electrodes. Normalized output power $P_{max}/(\Delta T)^2$ and maximum output current of 100 cycles in i-TE cell (Cu | Au | i-TE | Au | Cu, 15 × 15 × 1.8 mm) were shown in the inset. (**D**) Continuous thermal-charge/electrical-discharge process for the i-TE cell (Cu | Au | i-TE | Au | Cu, 15 × 15 × 1.8 mm, Au (40 nm) coated rough Cu foils) at the external resistor R = 5000 Ω and ΔT = 8 K. (**E**) Power of the continuous discharge process at the different external resistors and ΔT ~ 8 K. The inset showed the measurement circuit. (**F**) Corresponding energy density at the different external resistors. The energy was calculated by the integration of power to time (1 h) shown in Fig. E.

Fig. 4. Proof-of-concept of wearable i-TE device. (**A**) Tensile test of the i-TE material of Gelatin-0.8M KCl-0.42/0.25M $FeCN^{4-/3-}$ (r_v = 2.0), compared with the pure Gelatin. (**B**) Voltage generated from a proof-of-concept flexible i-TE wearable device with 25 unipolar elements (Cu | i-TE | Cu, 5 × 5 × 1.8 mm, smooth Cu foil) in series worn on the back of human hand. (**C**) Power (line, −), voltage (dash line, --), output current (dash dot line, -·-) curves of the proof-of-concept wearable i-TE device by harvesting the real body heat. (**D**) Performance comparison in output voltage and power of the wearable device by using e-TE materials and quasi-solid state i-TE materials under a real human body wearing condition. *N* represented the number of the n/p-typed thermoelectric elements in the wearable devices. The employed i-TE material was Gelatin-0.8M KCl-0.42/0.25M $FeCN^{4-/3-}$(r_v = 2.0).

Supplementary Materials for

Giant thermopower of ionic gelatin near room temperature

Cheng-Gong Han[1,3†], Xin Qian[2†], Qikai Li[1,6], Biao Deng[1], Yongbin Zhu[1], Zhijia Han[1], Wenqing Zhang[4], Weichao Wang[5], Shien-Ping Feng[6], Gang Chen[2*], Weishu Liu[1,3*]

[1]Department of Materials Science and Engineering, Southern University of Science and Technology, Shenzhen, Guangdong 518055, PR China

[2]Dapartment of Mechanical Engineering, Massachusetts Institute of Technology, Cambridge, MA 02139, USA

[3]Shenzhen Engineering Research Center for Novel Electronic Information Materials and Devices, Southern University of Science and Technology, Shenzhen 518055, China

[4]Department of Physics and Shenzhen Institute for Quantum Science & Technology, Southern University of Science and Technology, Shenzhen 518055, China

[5]Department of Electronics and Tianjin Key Laboratory of Photo-Electronic Thin Film Device and Technology, Nankai University, Tianjin 300071, China

[6]Department of Mechanical Engineering, The University of Hong Kong, Pokfulam, Hong Kong 999077, China

†: Equivalent contributions

*Email: liuws@sustech.edu.cn; gchen2@mit.edu

This file includes:

Materials and methods

Experimental methods

Materials. The raw materials are shown as follows: Gelatin (Photographic grade, B type, isoelectric point of *PI* = 4.9), $K_3Fe(CN)_6$ (*MW* = 329.25, ≥ 99.5%), $K_4Fe(CN)_6 \cdot 3H_2O$ (*MW* = 422.39, 99.0%) and NaCl (*MW* = 58.44, 99.5%), KOH (*MW* = 56.11, 95%) and K_2SO_4 (*MW* = 174.26, 99%) were purchased from Aladdin Industrial Corporation. KCl (*MW* = 74.55, 99.8%) and KNO_3 (*MW* = 101.1, 99%) were provided by Macklin Biochemical CO., Ltd. and Alfa Aesar, respectively. HCl (36 wt.% - 38 wt.%, GR) was purchased from Dongguan Dongjiang Chemical Reagent CO., Ltd. All chemical reagents were employed without further purification.

Preparation of quasi-solid state i-TE materials. The general formula of the as-fabricated i-TE materials was Gelatin-*x* MX-*m*/*n* $FeCN^{4-/3-}$ (MX = KCl, NaCl, KNO_3 and K_2SO_4, *x*: the molar concentration of MX salt; $FeCN^{4-/3-}$: $Fe(CN)_6^{4-}$/$Fe(CN)_6^{3-}$ of $K_4Fe(CN)_6/K_3Fe(CN)_6$; *m*: the molar concentration of $FeCN^{4-}$, *n*: the molar concentration of $FeCN^{3-}$). As an example, for preparing the i-TE material of Gelatin-0.8M KCl-0.42/0.25M $FeCN^{4-/3-}$, 6 ml distilled water (0.65 MΩ·cm) and 3 g gelatin were fixed firstly; then 0.3586 g KCl, 1.0752 g $K_4Fe(CN)_6 \cdot 3H_2O$ and 0.4964 g $K_3Fe(CN)_6$ were weighted according to the equation of $A = \frac{C \times V \times MW}{P}$, where *A*, *C*, *V*, *MW* and *P* were the amount, molar concentration, volume of distilled water, molar weight and purity, respectively. Additionally, 6, 7, 8, 9, 10 ml distilled water and 3 g gelatin were mixed to prepare the Gelatin-0.8M KCl-0.42/0.25M $FeCN^{4-/3-}$ with a series of volume ratio (r_v) of water to gelatin of 2.0, 2.3, 2.7, 3.0 and 3.3, respectively. The viscous and homogenous solution was obtained after magnetic stirring ~ 2 h at ~ 60 °C and then poured in a Teflon mould until the formation of the ionic gelatin-based quasi-solid state i-TE materials. The choice of *m*/*n* ratio was based on the experimental results with maximized positive thermopower. In the pH measurement of Gelatin-*x* KCl, the pH value was tuned in the solution before adding the gelatin, which *x* was always fixed at 0.8 M.

Fabrication of i-TE cell. Copper foils (10 μm thickness, Canrd Co.) were used as the electrodes for assembling the i-TE cell with a 1.8 mm-thick sandwich structure Cu | i-TE | Cu. In order to exclude the impact of the Cu-electrode corrosion to the thermopower, the Pt-sheet (size: 5 × 5 × 0.25 mm) and Au (40 nm) coated Cu foil (10 μm) were also employed as the electrodes. The Au coating on the Cu foil was deposited using MCIOOO ion sputter (Hitachi Ltd., Japan). It was found that the thermopower, measured by using Cu electrode, only showed small discrepancy within 6% compared with that using Au-coated Cu electrode. Considering the cost of experiments, Cu foils were used as the electrodes in all the subsequent measurements if without special explanation.

Performance characterization of i-TE materials. The thermopower measurement of the as-fabricated i-TE materials of Gelatin-*x* MX-*m*/*n* $FeCN^{4-/3-}$ (MX = KCl, NaCl, KNO_3 and K_2SO_4) was conducted on a homemade apparatus by using a single cell of Cu | i-TE | Cu (15 × 15 × 1.8 mm) encapsulated by a polyethylene film. The Keithley-2400 was used as the voltage meter, while the two commercial Peltier chips (Size: 4 × 4 cm) were used to generate the temperature difference. Two thermocouples were directly attached on the polyethylene film of the top and bottom surface of i-TE cell. A LabVIEW program was used for the temperature controlling and data acquisition of voltage and temperatures. The schematic and real images were provided in Fig. S13. For the measurement of discharging power and energy, the corresponding current-voltage curves were taken as the voltage reached to a near-saturation status. Here, we used a voltage varying rate < 0.3 mV min^{-1} to define the near-saturation status. Most the as-fabricated i-TE cells required 30 - 90 min to reach the near-saturation status at the first-time thermal charge process. In the discharge process, Keithley-2400 meter was used to obtain the current-voltage curves and hence the output power. The hysteresis loop of thermal stimulation and voltage response was obtained using the same setup. The temperature gradient was reversed from $+\Delta T$ to $-\Delta T$ (a sine wave change) during the cycling test, in which a $+\Delta T$ corresponded to a higher temperature of the upper electrode, vice versa. The temperature was controlled by monitoring the input of voltage and current into two commercial Peltier chips (Size: 4 × 4 cm), which was automatically controlled. The corresponding voltage signals were gathered by a Keithley-2400 meter when changing the ΔT. A quasi-continuous working mode was proposed and conducted under the constant temperature difference in the following manner: first thermal charging in open-circuit, discharging to 0 V in 10 s in short-circuit, and then thermally charged back to the high voltage in 3 or 1 min in open-circuit, i.e. a charge-discharge cycle. After long time discharge operation, the device can be reactivated by removing the temperature difference while short-circuiting two electrodes.

Characterizations. Cyclic voltammetry (CV) scanning from - 1 V to + 1 V was measured by using Zahner station (Zennium Pro., Germany), in which one platinum sheet was served as the working electrode while the other was employed as the counter and reference electrodes simultaneously. Electrochemical impedance spectroscopy (EIS) was adopted to characterize the resistances of the gelatin-based quasi-solid state i-TE material between 5×10^{-1} Hz and 1×10^{6} Hz at the AC amplitude of 10 mV. Herein, two platinum sheets (5 × 5 × 0.25 mm) were used as the electrodes of i-TE cell. The morphology of Cu foil was characterized by using the Scanning Electron Microscope (TESCAM MIRA3).

Thermal analysis of i-TE material. Thermal diffusivity (D_{th}) was measured by a laser flash method (LFA 467, Netzsch) and specific heat (C_P) was characterized by using Different Scanning Calorimetry (DSC 200F3, Netzsch) at 223-323 K. Thermal conductivity was calculated by using $\kappa = \rho D_{th} C_p$, which ρ represents the density.

Proof-of-concept wearable i-TE device. The proof-of-concept device was fabricated by using 25 i-TE single cells (5 × 5 × 1.8 mm) serially connected by conductive copper tape, which was encapsulated by a polyethylene film. The employed i-TE material was Gelatin-0.8M KCl-0.42/0.25M $FeCN^{4-/3-}$ (r_v = 2.0). One side of the device was closely pasted on the back of the hand for harvesting the body heat while the other side was exposed to the cold environment to obtain a temperature difference. The current-voltage curves and output power were read by the Keithley-2400 meter.

Sign convention of i-TE materials

Thermodiffusive thermopower works similar to thermoelectrics, but the current carriers are ions that cannot flow into electrodes. In fact, the thermodiffusive thermopower can be interpreted as the entropy transferred by the thermodiffusion of ions, similar to the case of thermoelectrics (49). Similar to the thermoelectrics, thermodiffusive thermopower is defined as the ratio between the electric field $-dV/dx$ and the temperature gradient dT/dx, which can be further written as:

$$S_{td} = -\frac{dV/dx}{dT/dx} = -\frac{V(T_H) - V(T_C)}{T_H - T_C} \quad (1)$$

where S_{td} is the thermodiffusive thermopower, V is the voltage, T_H and T_C are the temperatures at the hot electrode and the cold electrode, respectively. Eq (1) simply indicates that for a p-type thermodiffusive thermopower, the voltage is negative if the positive electrode is attached to the hot electrode.

On the other hand, thermopower can also arise from the redox reactions. In a thermogalvanic cell, a temperature gradient is imposed across the device, and the two electrodes are at different temperatures T_H and T_C. In this case, the final thermally induced voltage not only consists of thermodiffusion of the redox ions, but also the contribution from the temperature dependent standard electrode potential E^0 of redox couples, which will be more rigorously proved latter. Temperature dependence of the standard electrode potential E^0 is indeed referred as the "temperature coefficient" in electrochemistry. Temperature coefficient α_R is defined as the change of the standard electrode potential (E^0) with respect to temperature rise of an isothermal half-cell:

$$\alpha_R = \frac{dE^0}{dT} \tag{2}$$

For most of the thermogalvanic cells based on aqueous solutions, the thermodiffusive contribution to the voltage is on the order of (~ 10 μV K^{-1}) (34), much smaller than the temperature coefficient of redox couples (a few mV K^{-1}) (32). As this thermodiffusive thermopower can be negligible, the measured differential voltage of a thermogalvanic cell under a temperature difference can be written as:

$$\frac{V(T_H) - V(T_C)}{T_H - T_C} \approx \frac{E^0(T_H) - E^0(T_C)}{T_H - T_C} = \alpha_R \tag{3}$$

Eq. (3) is where the confusion arises and clearly the definition of temperature coefficient has opposite sign convention from the Seebeck coefficient. Note that Eq. (3) only holds when the thermodiffusion of redox couples is negligible, which is no longer the case in Gelatin- -0.42/0.25M $FeCN^{4-/3-}$, which will be discussed later. Temperature coefficient is also different from Seebeck coefficient in terms of the physical origin. It can be shown that the temperature coefficient is directly related to the redox entropy change:

$$\alpha_R = \frac{s_R - s_O}{nF} \tag{4}$$

where s_O and s_R are the molar entropy of the redox species in the redox reaction $O + ne \leftrightharpoons R$. Temperature coefficient is a thermodynamic property, which is fundamentally different from the thermodiffusive thermopower that is associated with ionic transport. Nevertheless, current literature often calls the thermopower measured of a thermogalvanic cell "Seebeck coefficient" (13,20,22), which consists of both thermodiffusive contribution and the redox reaction contribution, with the latter usually dominates. Such misnomer should be clarified. To further illustrate this, we recall one of the most investigated redox couple $FeCN^{4-/3-}$ (i.e., $Fe(CN)_6^{4-}/Fe(CN)_6^{3-}$). Since $FeCN^{4-}$ has more ordered hydration shell due to more charge thus lower solvation entropy compare with $FeCN^{3-}$ (35). The molar entropy of $FeCN^{4-}$ ($s_{FeCN^{4-}}$) is less than $FeCN^{3-}$ ($s_{FeCN^{3-}}$) and the temperature coefficient α_R is negative. For a thermogalvanic cell based on $FeCN^{4-/3-}$, according to the Eq. (3), a negative voltage difference would be obtained by attaching the positive electrode of the external meter to the hot side, i.e. $\Delta V = E^0(T_H) - E^0(T_C) < 0$. It actually produces the same sign of measured voltage as the p-type Seebeck coefficient by using same voltage meter connection. Due to the different sign conventions of the temperature coefficient and the thermodiffusive thermopower, a redox-

inert electrolyte with p-type thermodiffusive thermopower should be paired with a redox couple with negative temperature coefficient to achieve synergistic effect.

In this work, we use the word "thermopower" as a general term to describe the thermally differential voltage induced by either the thermodiffusion effect or the thermogalvanic effect, and clarify the sign conventions due to these two different mechanisms. Next, we will provide theoretical derivations showing that the thermodiffusion and electrochemical redox reaction can work synergistically, despite their fundamental differences.

Synergistic contribution of thermodiffusion and thermogalvanic effects to thermopower

In this section, we derive the synergistic contribution of thermodiffusion effect and thermogalvanic effect.

Thermodiffusive thermopower

In an electrolyte system, ionic flux and internal energy flux are described by Onsager relations (50):

$$J_i = L_{ii}\frac{\nabla(-\tilde{\mu}_i)}{T} + L_{iQ}\nabla\left(\frac{1}{T}\right) \tag{5}$$

$$J_Q = \sum_i L_{Qi}\frac{\nabla(-\tilde{\mu}_i)}{T} + L_{QQ}\nabla\left(\frac{1}{T}\right) \tag{6}$$

where J_i and $\tilde{\mu}_i$ are the ionic flux and electrochemical potential of the ion species i, respectively, J_Q is the heat flux across the sample, $L_{ii}, L_{iQ}, L_{Qi}, L_{QQ}$ are the transport coefficients and T is the temperature. Onsager reciprocity ensures $L_{Qi} = L_{iQ}$. Note that the electrochemical potential is defined as $\tilde{\mu}_i = \mu_i[n_i(r), T(r)] + q_i V$, where the chemical potential μ_i is a functional of concentration profile $n_i(r)$ and temperature profile $T(r)$. The gradient of electrochemical potential is therefore:

$$\nabla\tilde{\mu}_i = \left(\frac{\partial\mu_i}{\partial n_i}\right)_T \nabla n_i + \left(\frac{\partial\mu_i}{\partial T}\right)_{n_i} \nabla T + q_i\nabla V \tag{7}$$

The subscripts denote that the variable held constant when taking the partial derivatives. From Maxwell's relation, the partial derivative of free energy with respect concentration is the partial entropy s_i, i.e.:

$$\left(\frac{\partial\mu_i}{\partial T}\right)_{n_i} = -\left(\frac{\partial S}{\partial n_i}\right)_T = -s_i \tag{8}$$

where S is the total entropy of the solution. In an ideal solution, the chemical potential is related to pure system of i through $\mu_i = \mu_i^{pure} + k_B T\, ln\, ln\, \frac{n_i}{N}$, where N is the total number of molecules, μ_i^{pure} is the chemical potential of the system of pure n_i. We can therefore derive the partial derivative:

$$\frac{\partial \mu_i}{\partial n_i} = \frac{k_B T}{n_i} \tag{9}$$

Then the electrochemical potential is simplified to the following expression:

$$\nabla \tilde{\mu}_i = \frac{k_B T}{n_i} \nabla n_i - s_i \nabla T + q_i \nabla V \tag{10}$$

Plug the above equation back to Eq. (5), we now explicitly relate ionic flux to the electric field and the temperature gradient as follows:

$$J_i = L_{ii} \left(-\frac{k_B}{n_i} \nabla n_i - \frac{q_i}{T} \nabla V + \frac{s_i}{T} \nabla T - \frac{\bar{\bar{S}}_i}{T} \nabla T \right) \tag{11}$$

where $\bar{\bar{S}}_i$ is the transported entropy along with the ionic species i, defined as

$$\bar{\bar{S}}_i = \frac{1}{T} \frac{L_{Qi}}{L_{ii}} \tag{12}$$

The Onsager coefficient $L_{ii} = \frac{n_i D_i}{k_B}$ where D_i is the diffusion coefficient, then we finally have the expression of ionic flux:

$$J_i = -D_i \left(\nabla n_i + \frac{q_i n_i}{k_B T} \nabla V + \frac{\hat{S}_i n_i}{k_B T} \nabla T \right) \tag{13}$$

where $\hat{S}_i = \bar{\bar{S}}_i - s_i$ is referred as the Eastman entropy of transfer (51), where s_i is the partial entropy of ion species.

In open circuit condition, there is no net current carried by ions, then:

$$\sum_i q_i J_i = 0 \tag{14}$$

Therefore, we have:

$$-\sum_{\mathrm{i}} D_i \cdot \left(q_i \nabla n_i + \frac{q_i^2 n_i}{k_B T} \nabla V + \frac{q_i \hat{S}_i n_i}{k_B T} \nabla T \right) = 0 \tag{15}$$

If we assume near equilibrium, such that concentration profile can be approximated as $n_i(r) = n_i^0 + \delta n_i(r)$, where $\delta n_i \ll n_i^0$, then Eq. (15) is approximately:

$$-\sum_{i} q_i D_i \left(\nabla(\delta n_i) + \frac{q_i n_i^0}{k_B T} \nabla V + \frac{\hat{S}_i n_i^0}{k_B T} \nabla T \right) = 0 \tag{16}$$

In the near equilibrium regime, ΔV and ΔT across the device are small enough such that:

$$\frac{q_i \Delta V}{k_B T} \ll \frac{n_i^0}{\delta n_i}, \qquad \frac{\hat{S}_i \Delta T}{k_B T} \ll \frac{n_i^0}{\delta n_i} \tag{17}$$

then we can neglect the term $\nabla(\delta n_i)$ and Eq. (16) can be simplified as:

$$\sum_{\mathrm{i}} \left(\frac{q_i^2 n_i^0 D_i}{k_B T} \nabla V + \frac{q_i n_i^0 \hat{S}_i D_i}{k_B T} \nabla T \right) = 0 \tag{18}$$

Therefore, the temperature gradient and electrostatic potential gradient are related as:

$$\nabla V = -\frac{\sum_{\mathrm{i}} q_i n_i^0 \hat{S}_i D_i}{\sum_{\mathrm{i}} q_i^2 n_i^0 D_i} \nabla T \tag{19}$$

Therefore, the thermodiffusive thermopower is derived as:

$$S_{td} = \frac{\sum_{\mathrm{i}} q_i n_i^0 \hat{S}_i D_i}{\sum_{\mathrm{i}} q_i^2 n_i^0 D_i} \tag{20}$$

Here we adopted the same sign convention as Seebeck coefficient for e-TE materials.

In the case of a symmetrical electrolyte like KCl with ($n_+^0 = n_-^0$), Eq. (20) can be simplified to:

$$S_{td} = \frac{\left(\hat{S}_+ D_+\right) - \left(\hat{S}_- D_-\right)}{e(D_+ + D_-)} \tag{21}$$

From Eq. (13), without electric field and concentration gradient, the thermally driven ionic flux is simply $J_i = -n_i \frac{D_i \hat{S}_i}{k_B T} \nabla T$. If we relate ionic flux to "thermodiffusion velocity" v_i^T through $J_i = -n_i v_i^T$, then we have derived

the relation between thermodiffusion velocity and the temperature gradient $-\nabla T$ as $v_i^T = \frac{D_i \hat{S}_i}{k_B T}(-\nabla T)$. Therefore we can define the thermal mobility μ_i^T as:

$$\mu_i^T = \frac{D_i \hat{S}_i}{k_B T} \tag{22}$$

Eq. (22) is essentially the Einstein's relation for thermodiffusion. With the ionic mobility defined as $\mu_i^I = \frac{D_i}{k_B T}$, Eastman entropy of transfer is essentially the ratio between thermal mobility and ionic mobility.

Further, charge mobility of ions is defined as:

$$\mu_i^q = \frac{q_i D_i}{k_B T} \tag{23}$$

Eq. (21) can be further re-written in a simpler form:

$$S_{td} = \frac{\mu_+^T - \mu_-^T}{\mu_+^q + \mu_-^q} \tag{24}$$

Therefore, we can see that the difference in thermal mobilities of the cations and anions determines the sign of the thermopower, and the thermal mobility is simultaneously determined by diffusion coefficient D and the Eastman entropy of transfer $\hat{S}$.

Coupling between thermodiffusion effect and thermogalvanic effect

However, the experiment measuring the voltage drop across the Gelatin-*x* KCl-*m*/*n* $FeCN^{4-/3-}$ sample does not simply measure S_{td} when some of the ionic species ($FeCN^{4-/3-}$) are electrochemically active. The redox reactions at the electrode interface will affect the electrochemical potential of electrons in the electrode. In this case, we need to consider the redox reaction:

$$O + ne \leftrightharpoons R \tag{25}$$

where O is the oxidized species, R is the reduced species. In Gelatin-0.42/0.25M $FeCN^{4-/3-}$ samples, O is $FeCN^{3-}$ and R is $FeCN^{4-}$. At the equilibrium, the net change in electrochemical potential should be zero at both the hot electrode and the cold electrode:

$$\begin{matrix}\tilde{\mu}_O(T_H) + n\tilde{\mu}_e(T_H) = \tilde{\mu}_R(T_H) \\ \tilde{\mu}_O(T_C) + n\tilde{\mu}_e(T_C) = \tilde{\mu}_R(T_C)\end{matrix} \quad (26)$$

where electrochemical potential of the species O and R, $\tilde{\mu}_i = \mu_i + q_i V$ $(i = O, R)$, contains the chemical potential part μ_i and electrostatic potential part $q_i V$, where q_i is the charge of species i and V is the electrostatic potential in the electrolyte. $\tilde{\mu}_e = E_F - FV_e$ is the electrochemical potential per mole of electrons, where E_F is the Fermi level of electrode, and V_e is the electrostatic potential in the electrode. Since the Fermi level E_F can be regarded as a constant in the metal electrode, the difference of electrochemical potential between the hot and cold sides is directly the voltage difference. Now we take the difference of electrochemical potential between the hot side and the cold side:

$$\begin{aligned} n\Delta\tilde{\mu}_e = \Delta\tilde{\mu}_R - \Delta\tilde{\mu}_O = (\Delta\mu_R - \Delta\mu_O) + q_R\Delta V - q_O\Delta V = \left(\frac{\partial\mu_R}{\partial T} - \frac{\partial\mu_O}{\partial T}\right)\Delta T + (q_R - q_O)\Delta V \\ = -(s_R - s_O)\Delta T + (-nF)(-S_{td}\Delta T) \end{aligned} \quad (27)$$

where the differential operator Δ means the quantity at the hot side minus the quantity at the cold side. For the last equality in Eq. (27), we have used the relations $\frac{\partial\mu_i}{\partial T} = -s_i$ and $S_{td} = -\frac{\Delta V}{\Delta T}$, charge conservation $q_R - q_O = -nF$ for each mole of reactions, where F is the Faraday constant.

Therefore, the measured thermopower is:

$$S_i = \frac{\Delta\tilde{\mu}_e}{nF\Delta T} = -\frac{\Delta V_e}{\Delta T} = -\frac{s_R - s_O}{nF} + S_{td} \quad (28)$$

We can further simplify Eq. (28) by relating the first term to the temperature coefficient of redox couples. The temperature coefficient of the redox reaction in Eq. (25) is written as:

$$\alpha_R = \frac{\Delta s_r}{nF} = \frac{s_R - s_O}{nF} \quad (29)$$

where $\Delta s_r = s_R - s_O$ is the entropy change (entropy of the reduced species minus the oxidized species) in the standard reduction reaction $O + ne \leftrightharpoons R$. We further define the partial thermodiffusive thermopower of species i as

$$S_{td}(i) = \frac{q_i n_i \left(\hat{S}_i D_i\right)}{\sum_i q_i^2 n_i D_i} \tag{30}$$

Then total thermopower can therefore be written as a sum over different ionic species:

$$S_i = -\alpha_R + \sum_i S_{td}(i) \tag{31}$$

Eq. (31) is the key theoretical result in this analysis, showing that different mechanisms can synergistically contribute to thermopower. **The negative sign in front of the temperature coefficient α_R shows that a p-type thermodiffusive thermopower should be paired with a redox couple with negative temperature coefficient.**

Specific contribution to thermopower

According Eq. (31), the thermopower of the Gelatin-0.8M KCl-0.42/0.25M $FeCN^{4-/3-}$ (r_v = 2.0) sample can therefore be separated into different parts:

$$S_i = -\alpha_R + S_{td}\left(K^+ - FeCN^{4-/3-}\right) + S_{td}(KCl) + S_{td}(gelatin) \tag{32}$$

where $S_{td}(gelatin)$ is the intrinsic thermopower of gelatin 1.3 mV K^{-1}.

To separately determine the redox contribution to the thermopower, i.e. $-\alpha_R$, we need to eliminate the effect of the temperature gradient such that $S_{td}(\mathrm{FeCN}^{4-/3-})$ is zero. To achieve this, we use a three-electrode set-up, with Pt as working electrode and a SCE (saturated calomel electrode) as reference and counter electrodes in Gelatin-$FeCN^{4-/3-}$ (x = 0 M, m/n = 0.42/0.25 M, r_v = 2.0) system (Fig. 2D). Then we apply homogeneous heating to increase the temperature of the system and the open circuit voltage (V_{oc}) is measured as a function of temperature. In this way, we solely measure the relative temperature coefficient of standard reduction potential of $FeCN^{4-/3-}$ with respect to an SCE:

$$\alpha_{FeCN\ vs\ SCE} = \frac{1}{\Delta T}\left[\left(E^0_{FeCN}(T+\Delta T) - E^0_{SCE}(T+\Delta T)\right) - \left(E^0_{FeCN}(T) - E^0_{SCE}(T)\right)\right] \tag{33}$$

In the thermogalvanic cell, the temperature coefficient is the first-order derivative of standard electrode potential with respect to temperature:

$$\alpha_R = \frac{1}{\Delta T}[E^0_{FeCN}(T+\Delta T) - E^0_{FeCN}(T)] \quad (34)$$

Since we are measuring with respect to SCE, Eq. (34) is further written as:

$$\alpha_R = \frac{1}{\Delta T}\left[\left(E^0_{FeCN}(T+\Delta T) - E^0_{SCE}(T+\Delta T)\right) - \left(E^0_{FeCN}(T) - E^0_{SCE}(T)\right) + (E^0_{SCE}(T+\Delta T) - E^0_{SCE}(T))\right] \quad (35)$$

Therefore, the entropy change is expressed as:

$$\alpha_R = \alpha_{FeCN\ vs\ SCE} + \alpha^0_{SCE} \quad (36)$$

where $\alpha^0_{SCE} = (E^0_{SCE}(T+\Delta T) - E^0_{SCE}(T))/\Delta T$ is the temperature coefficient of SCE. The relative temperature coefficient with respect to SCE is measured to be -1.8 mV K^{-1} as shown in Fig. S11. Note that the temperature coefficient of SCE is -0.468 mV K^{-1} (31), therefore the temperature coefficient of $FeCN^{4-/3-}$ in gelatin is -2.27 mV K^{-1}, which is ~ 60% larger than that in aqueous solution of $FeCN^{4-/3-}$ possibly due to different water structure near the polymer network (35,42,52). For the Gelatin-$FeCN^{4-/3-}$ sample, the gelatin itself contributed 1.3 mV K^{-1} while the total thermopower is measured to be 4.8 mV K^{-1}, we can derive that the thermodiffusion of K^+ and $FeCN^{4-/3-}$ contributed 1.23 mV K^{-1}, in Gelatin-$FeCN^{4-/3-}$. Finally after adding KCl (x = 0.8 M, r_v = 2.0) into the gelatin electrolyte, the total thermopower is observed to increased to 12.7 mV K^{-1}, therefore thermodiffusion of KCl contributed 7.9 mV K^{-1}. We summarize the contributions from thermogalvanic effect, thermodiffusion effect in Fig. 2G (gelatin 10.2% (S_{td} = 1.3 mV K^{-1}), thermogalvanic effect of $FeCN^{4-/3-}$ 17.9% ($-\alpha_R$ = 2.27 mV K^{-1}), thermodiffusion of $K_3Fe(CN)_6$ and $K_4Fe(CN)_6$ 9.7% (S_{td} = 1.23 mV K^{-1}), thermodiffusion of KCl 62.2% (S_{td} = 7.9 mV K^{-1})). Note that the thermopower of Gelatin-0.8M KCl is measured as 6.7 mV K^{-1}, smaller than the 7.9 mV K^{-1} estimated above, which might be due to the fact that ionization of -COOH groups is dependent on concentration of the added ionic species, thereby affecting the Eastman entropy of transfer of K^+ and Cl^-. However, the above estimation at least provided a qualitative description of the relative contribution from different mechanisms.

Efficiency of i-TE device

Thermal transport property is a significant aspect for i-TE materials because the thermal-to-electric conversion performance is based on the establishment of temperature differences. To measure the thermal conductivity, we first measure the thermal diffusivity (Fig. S7 A) using laser flash method (LFA, Netzsch) between 290 K and 320 K. Then specific heat of the gelatin was measured using DSC, and the increased specific heat above 273 K was observed for the gelatin sample (Fig. S7 B). Thermal conductivity was finally obtained using the thermal diffusivity and specific heat, which increases as increasing temperature (Fig. S7 C). The lowest thermal conductivity, 0.15 W m^{-1} K^{-1} at 293 K, was observed for the Gelatin-0.8M KCl-0.42/0.25M $FeCN^{4-/3-}$ (r_v = 2.0), indicating easy establishment of the temperature gradient.

In e-TE and thermogalvanic cells, the figure-of-merit is often used as it determines the maximum efficiency of device:

$$Z_i T = \frac{S_i^2 \sigma}{\kappa} T \tag{37}$$

where S_i, σ, κ and T were the thermopower, ionic conductivity, thermal conductivity and absolute temperature, respectively. However, such ZT definition is not valid for our device because the as-fabricated i-TE device works in a transient manner, which makes its working principle be different from the conventional e-TE material. This is essentially due to the fact that thermodiffusion induced voltage is capacitive in nature and the relatively slow migration of redox couples crosses the material due to the low diffusion coefficient.

The heat-to-electrical conversion efficiency (η) relative to Carnot efficiency (η_{Carnot}) for the i-TE device could be expressed by the following equation:

$$\eta_r = \frac{\eta}{\eta_{Carnot}} = \frac{\int_0^{\tau_{dis}} V(t)\cdot I(t) dt}{\lambda \frac{\Delta T}{d} \cdot A \cdot (\tau_{ch}+\tau_{dis})} \div \left(\frac{\Delta T}{T_H}\right) = \frac{\tau_{dis}}{\tau_{ch}+\tau_{dis}} \frac{P_{ave}}{(\Delta T)^2} T_H \frac{d}{\lambda} \tag{38}$$

where $V(t)$ and $I(t)$ are the voltage and current during the discharge with fixed resistance, A, d, λ, P_{ave} and T_H represent the area and thickness of the quasi-solid state i-TE material, thermal conductivity, average power density during the discharge time and the high-side temperature, respectively. A prefactor $\frac{\tau_{dis}}{\tau_{ch}+\tau_{dis}}$ appears in Eq. (38) as compared with efficiency calculation of other thermogalvanic systems (9,22) since our system works

transiently, where τ_{dis} is the electrical discharge time and τ_{ch} is the thermal charge time. The as-fabricated i-TE cell discharged to a constant resistance R = 5000 Ω at ΔT = 8 K, the corresponding relatively conversion efficiency was around η_r = 0.01% (τ_{ch} = 42 min, τ_{dis}= 60 min) (Fig. 3D). Based on such discharge test, the efficiency we obtained in as-demo single i-TE cell by using body heat is normalized around η_r = 0.006%. The low conversion efficiency is attributed to smaller temperature difference, the relatively long charging time and the relatively lower output power density compared with the liquid based i-TE device. Some promising strategies are shown as follows to improve the energy conversion efficiency.

(1) Optimizing the electrode design.

The surface area of electrodes is important for the capacitance characteristic as well as the redox reactions. Indeed, R. Baughman's group reported a significantly increased output current thereby the output power by using activated carbon cloth electrode in the thermogalvanic cell ($K_3Fe(CN)_6/(NH_4)_4Fe(CN)_6$ redox couple) (21). In our work, a near one order of output power due to the increase of output current was observed when replacing the Cu foil with smooth surface by 40 nm Au coated Cu foil with rough surface. We have not focused on optimizing the electrodes in this study. Further work in this direction can be fruitful.

(2) Reducing the thermal charge time.

It was found that the thermal charge time could be reduced from 3 min to roughly 20 seconds by changing the cell from single layer to three layers. Theoretically, the thermal charge time could be reduced by a factor of N^2, where N is the ratio of thickness reduction. We also could directly reduce layer thickness. This could be a direct way to boost the energy conversion efficiency in the quasi-continuous thermal-charge/electrical-discharge process.

(3) Decreasing the thermal loss.

In our current proof-of-concept wearable device, only the as-fabricated i-TE elements were used to connect in series by the conductive copper tape, which could result in a large amount of heat loss, since the thermal conductivity of copper was 3 order magnitudes higher than the as-fabricated i-TE materials.

(4) Further optimizing the i-TE materials.

Not only p-type i-TE materials presented in this work, n-type i-TE materials are also desirable. The strategy using synergistic thermodiffusion and thermogalvanic effects can be also applied to achieve n-type i-TE materials for further improving the device voltage with paired n-type and p-type i-TE materials.

Finally, it is worthy to point out that the well-matched voltage and output power with the sensors in IoT seem to be more important than the conversion efficiency for many practical applications of wearable electric devices. The high thermopower of i-TE materials makes it easy to produce high voltage with only a small number of legs that can be matched to IoT sensors, as we have shown in this paper. This is a significant advantage compared to e-TE devices.

Reactivation of the i-TE cell

In this section, we discuss the mechanism how the cell can be reactivated after a long-time thermal charge and electrical discharge service, by removing the temperature gradient and short-circuiting two electrodes.

Operation cycle of the i-TE cell (Gelatin-*x* KCl-*m*/*n* $FeCN^{4-/3-}$) is shown in Fig. S14. Initially, all the mobile ions K^+, Cl^-, H^+, $FeCN^{4-}$ and $FeCN^{3-}$ are distributed homogenously in the as-fabricated i-TE material of Gelatin-*x* KCl-*m*/*n* $FeCN^{4-/3-}$, and there is no electromotive forces for current. In the thermal charge process, a temperature difference is applied across the cell. Because of the mismatch in thermal mobility ($\mu_i^T = \frac{D_i \hat{S}_i}{k_B T}$) of cations and anions, there will be more K^+ accumulated on the cold side compared with Cl^-, resulting in net positive and negative charge density near the cold and hot electrode, respectively. Such net charge density profile induces a build-in electric field pointing from cold side to the hot side, generating the voltage. Meanwhile, the electrochemical redox couple $FeCN^{3-}$ and $FeCN^{4-}$ would also shift electrochemical potential of the cold and hot electrodes due to the temperature difference, working synergistically with the thermodiffusion effect. In the electrical discharge process, electrons will flow from the hot electrode to the cold electrode. Such current contains capacitive (non-Faradic) current due to coupling with the ion provider KCl and a faradaic current due to the redox couple $FeCN^{4-/3-}$. The non-Faradaic current would result in the polarization of the electrode, such that net negative charges would accumulate on the cold electrode surface, while positive charges would accumulate on the hot electrode surface. Such increase in net surface charges (i.e. polarization of the electrode) would facilitate the physical adsorption of the counterions. Namely, more K^+ would be adsorbed to the cold

electrode surface as the discharging process proceeds, especially after the cell quasi-continuously discharged for many cycles. However, K^+ and Cl^- are redox-inert ions, and adsorption would result in the slower kinetics, thereby suppressing the redox reaction rate (53). This could possibly explain why the current and output power decay after many cycles of quasi-continuous discharge as shown in Fig 3C of the maintext. Nonetheless, such decayed power due to the electrode polarization can be easily solved by the reactivation process. During the reactivation, the i-TE cell is cooled down by removing the temperature gradient, such that the concentration profiles of ions are relaxed to homogeneous distribution. Further to depolarize the two electrodes, we short-circuit them while cooling down the cell. Then the accumulated electrons on the cold electrode flow back into the hot electrode, and the cell returns to the initial state.

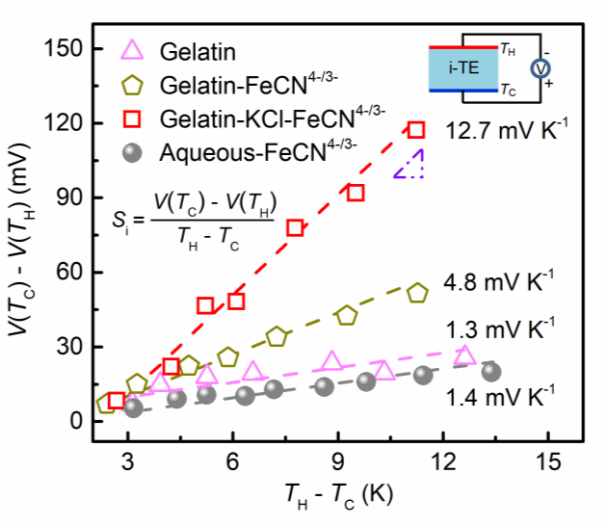

Fig. S1. Thermopower measurement of the i-TE materials of Gelatin-*x* KCl-*m*/*n* $FeCN^{4-/3-}$: Gelatin (pure gelatin gel), Gelatin-$FeCN^{4-/3-}$ (*x* = 0 M, *m*/*n* = 0.42/0.25 M), Gelatin-KCl-$FeCN^{4-/3-}$ (*x* = 0.8 M, *m*/*n* = 0.42/0.25 M), aqueous-$FeCN^{4-/3-}$ (*m*/*n* = 0.42/0.25 M). Cu foils with smooth surface were employed as electrodes. $V(T_C)$ -$V(T_H)$ is the voltage difference, while $T_H - T_C$ is the temperature difference. In the voltage measurement, the positive electrode of the voltage meter is connected to the cold side shown in the inset, which is consistent with commercially available Seebeck coefficient measurement. The thermopower S_i is determined by the slope of voltage difference versus temperature difference, i.e. $S_i = -\frac{V(T_H)-V(T_C)}{T_H-T_C} = \frac{V(T_C)-V(T_H)}{T_H-T_C}$.

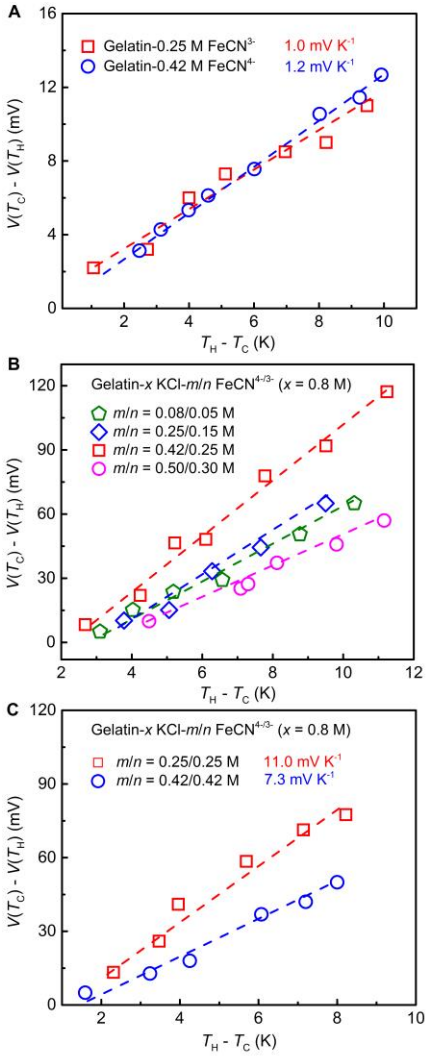

Fig. S2. Thermopower measurement for the i-TE materials of (**A**) Gelatin-*m* $FeCN^{4-}$ (*m* = 0.42 M) and Gelatin-*n* $FeCN^{3-}$ (*n* = 0.25 M), (**B**) Gelatin- 0.8M KCl-*m*/*n* $FeCN^{4-/3-}$ (*m*/*n* = 0.08/0.05, 0.25/0.15, 0.42/0.25 and 0.50/0.30 M) (Cu | i-TE | Cu), (**C**) Gelatin- 0.8M KCl-*m*/*n* $FeCN^{4-/3-}$ (*m*/*n* = 0.25/0.25 M and 0.42/0.42 M) (Cu | i-TE | Cu). The Cu foils with smooth surface were employed as electrodes. The $V(T_C) - V(T_H)$ is the voltage difference, while the $T_H - T_C$ is the temperature difference.

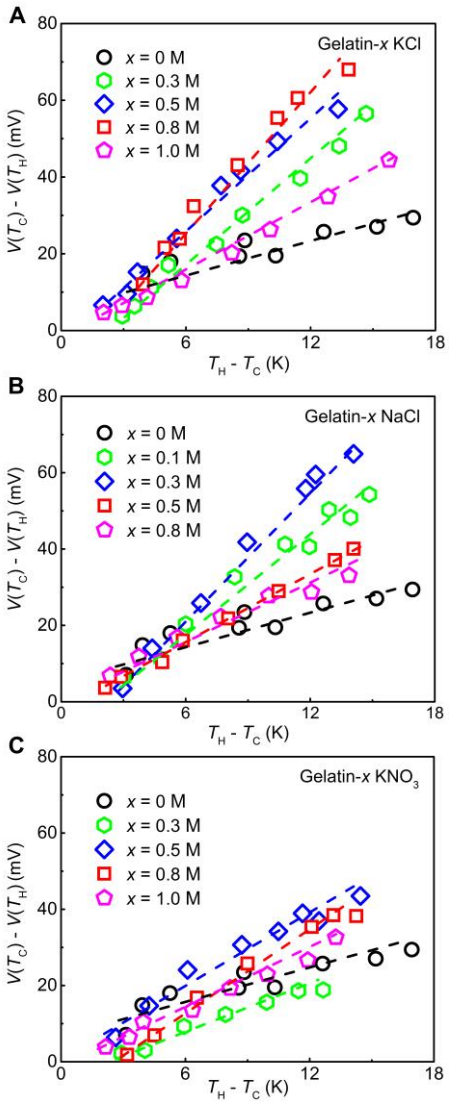

Fig. S3. Thermopower measurement for the i-TE materials of (**A**) Gelatin-*x* KCl, (**B**) Gelatin-*x* NaCl, and (**C**) Gelatin-*x* KNO_3 with the concentration of x = 0, 0.1, 0.3, 0.5, 0.8, 1.0 M. The $V(T_C) - V(T_H)$ is the voltage difference, while the $T_H - T_C$ is the temperature difference.

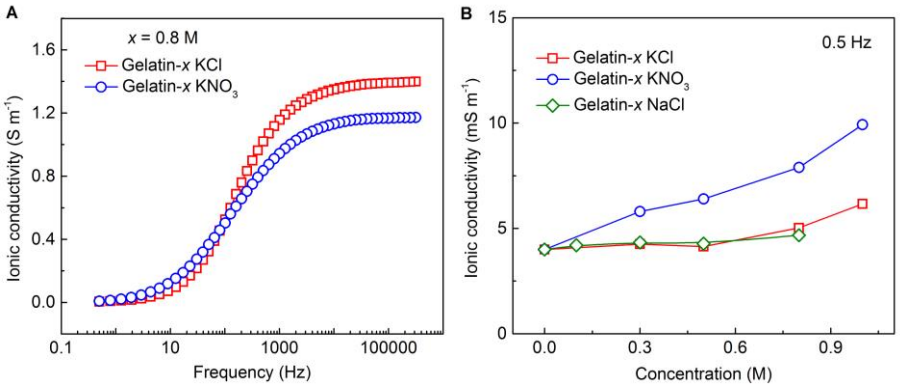

Fig. S4. (**A**) Frequency dependent ionic conductivity of the i-TE materials of Gelatin- 0.8M KCl and Gelatin- 0.8M KNO_3. (**B**) Concentration dependent ionic conductivity of the i-TE materials of Gelatin-*x* KCl, Gelatin-*x* KNO_3 and Gelatin-0.8M NaCl at 0.5 Hz. The ionic conductivity was calculated by the real part of the impedance in the Nyquist plot of electrochemical impedance spectroscopy (Zahner station, Zennium Pro., Germany).

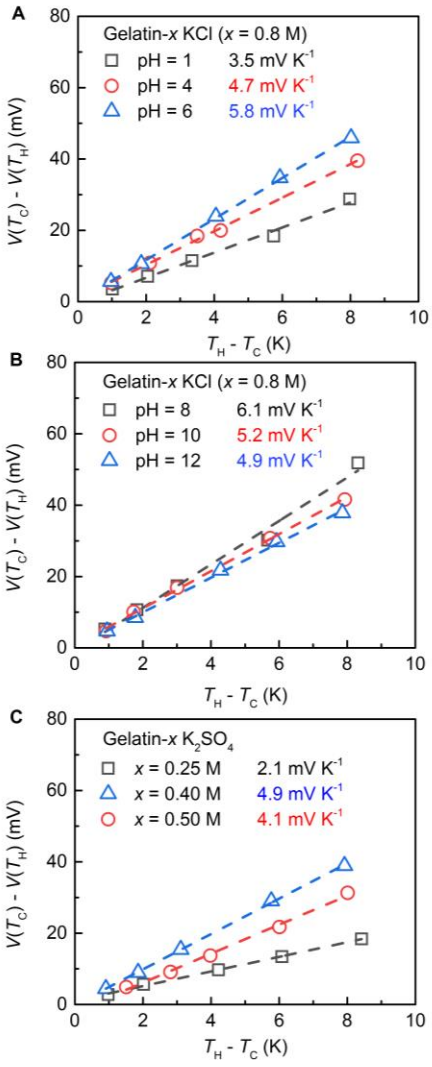

Fig. S5. Thermopower measurement for the i-TE materials of Gelatin- 0.8 M KCl (x = 0.8 M) (**A**) pH < 7, (**B**) pH > 7. (**C**) Gelatin-x K_2SO_4 (x = 0.25, 0.40, 0.50 M). The $V(T_C) - V(T_H)$ is the voltage difference, while the $T_H - T_C$ is the temperature difference. pH < 7 and pH > 7 were tuned by HCl and KOH, respectively.

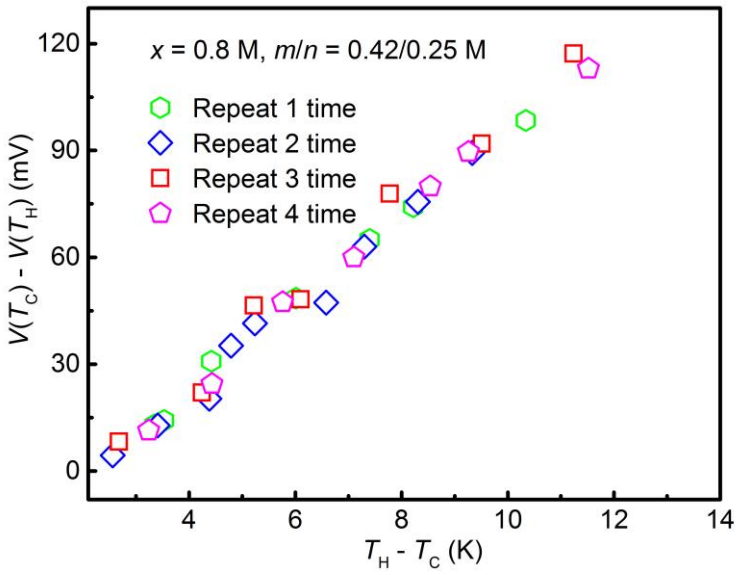

Fig. S6. Four independent measurements of the thermopower for the i-TE materials of Gelatin-0.8M KCl-0.42/0.25M $FeCN^{4-/3-}$ (r_v = 2.0)) showing a good consistency and repeatability. The $V(T_C) - V(T_H)$ is the voltage difference, while the $T_H - T_C$ is the temperature difference.

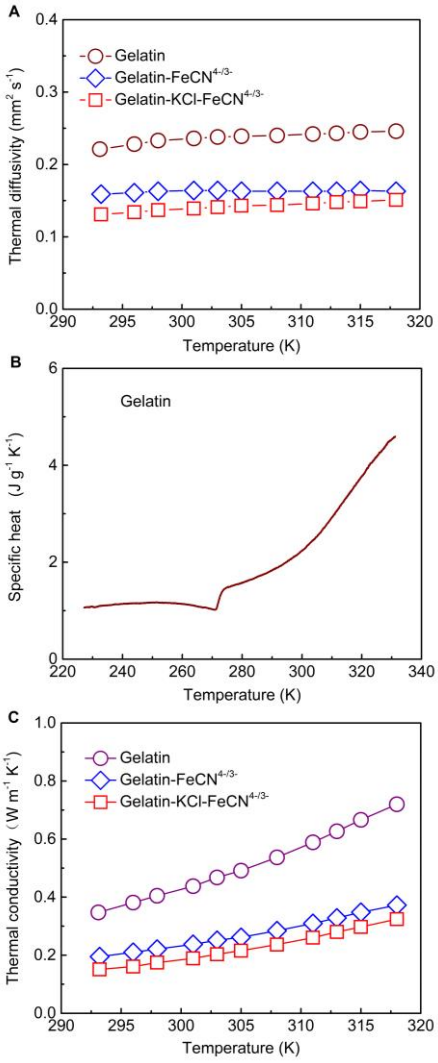

Fig. S7. The thermal properties of the i-TE material of Gelatin-*x* KCl-*m*/*n* FeCN$^{4-/3-}$, including Gelatin (*x* = 0 M, *m*/*n* = 0 M), Gelatin-FeCN$^{4-/3-}$ (*x* = 0 M, *m*/*n* = 0.42/0.25 M) and Gelatin-KCl-FeCN$^{4-/3-}$ (*x* = 0.8 M, *m*/*n* = 0.42/0.25 M), (**A**) thermal diffusivity, (**B**) specific heat of gelatin, (**C**) thermal conductivity calculated by using thermal diffusivity and specific heat of gelatin matrix.

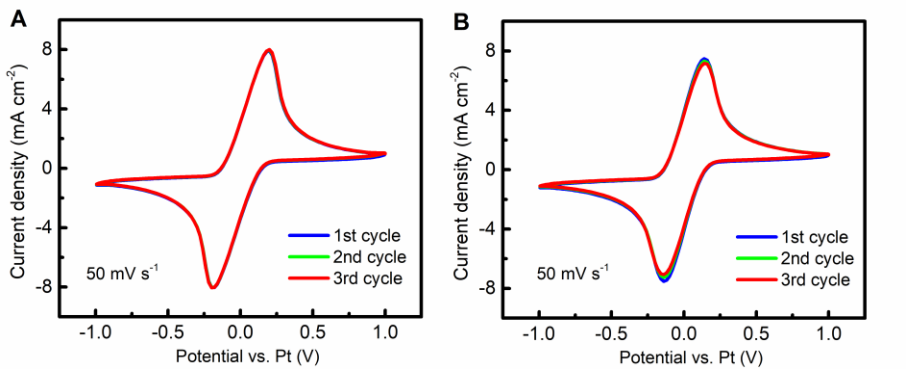

Fig. S8. Cyclic voltammetry (CV) curves scanned at 50 mV s^{-1} for (**A**) Gelatin-0.42/0.25M $FeCN^{4-/3-}$ and (**B**) Gelatin-0.8M KCl-0.42/0.25M $FeCN^{4-/3-}$.

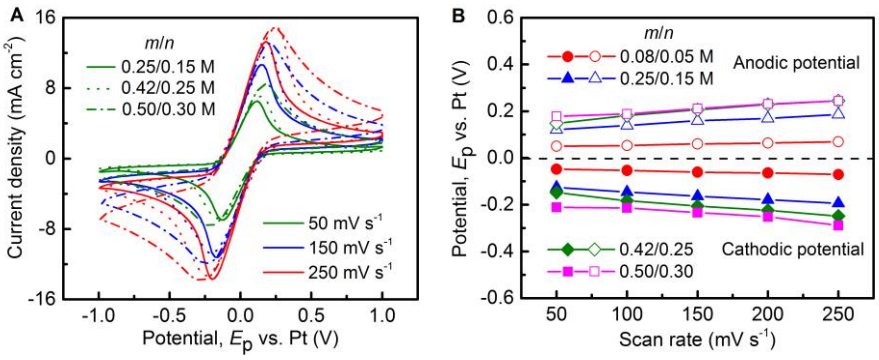

Fig. S9. (**A**) Cyclic voltammetry (CV) curves of the i-TE materials of Gelatin- 0.8M KCl-*m*/*n* $FeCN^{4-/3-}$ (*m*/*n* = 0.08/0.05, 0.25/0.15, 0.42/0.25 and 0.50/0.30 M), scanned at 50, 150 and 250 mV s^{-1}. (**B**) Corresponding potential of the cathodic and anodic peaks scanned at different speeds.

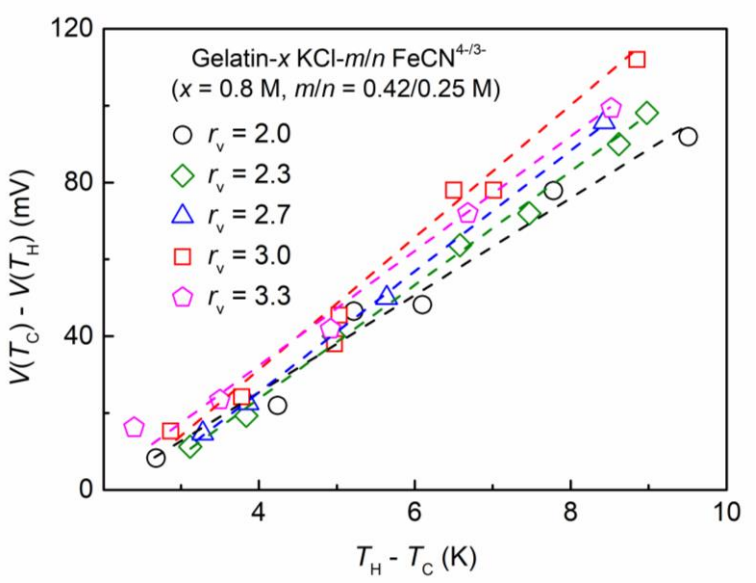

Fig. S10. Thermopower measurement for the i-TE materials of Gelatin-0.8M KCl-0.42/0.25M $FeCN^{4-/3-}$ (Cu | i-TE | Cu) at the various volume ratio (r_v) of water to gelatin. The Cu foils with smooth surface were employed as electrodes.

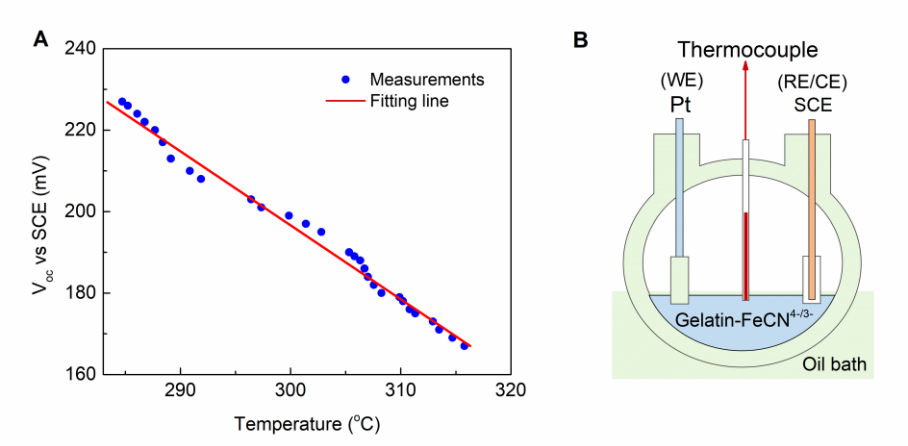

Fig. S11. (**A**) Open-circuit voltage vs. SCE (saturated calomel electrode) with the dependent of temperature in an isothermal three-electrode system. (B) Isothermal three-electrode system for Gelatin- -0.42/0.25M*n* $FeCN^{4-/3-}$ (r_v = 2.0). Pt is served as work electrode (WE), while SCE is used as reference electrode (RE) and counter electrode (CE). Temperature coefficient relative to SCE extracted by linear fitting is -1.8 mV K^{-1} vs. SCE. Note that the SCE itself has a temperature coefficient of -0.47 mV K^{-1} (31), therefore the temperature coefficient of $FeCN^{4-/3-}$ is -2.27 mV K^{-1}. In electrochemistry, the temperature dependence of the standard electrode potential (E^0), as an isothermal quantity, is referred as "temperature coefficient", which is defined as $\alpha_R = dE^0/dT$.

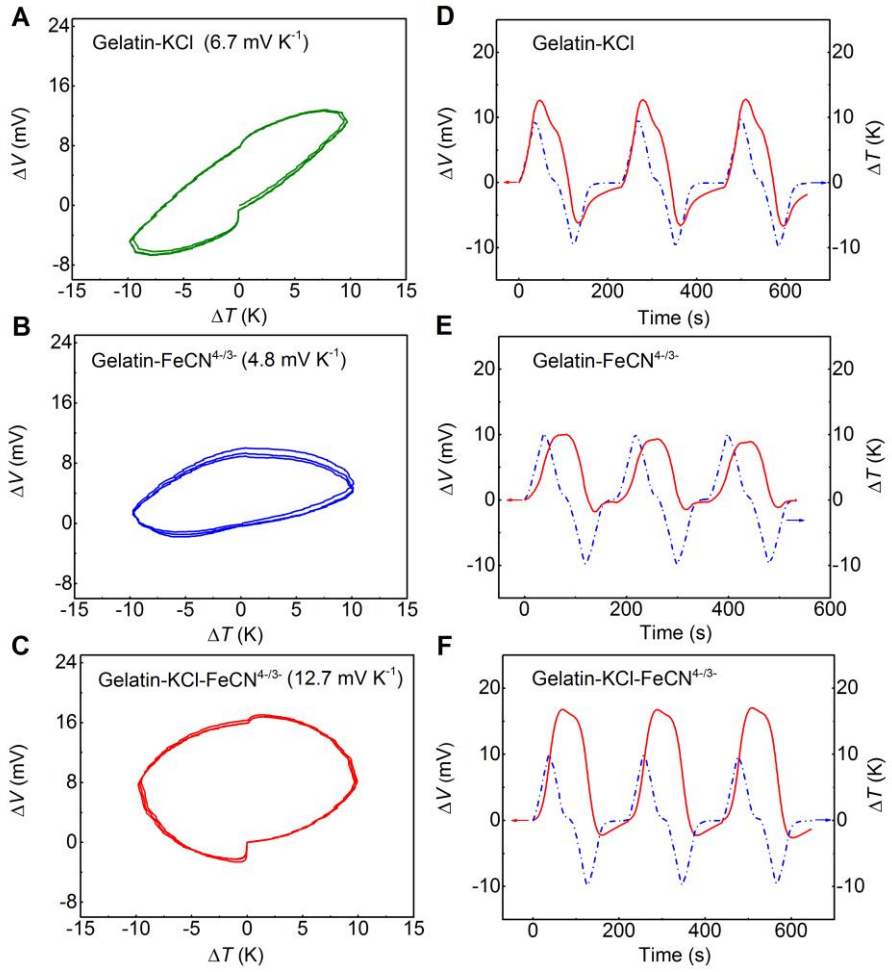

Fig. S12. The hysteresis loop of thermal simulation and electric response for the i-TE material Gelatin-*x* KCl-*m*/*n* $FeCN^{4-/3-}$: (**A**) Gelatin-KCl (*x* = 0.8 M, *m*/*n* = 0 M), (**B**) Gelatin-$FeCN^{4-/3-}$ (*x* = 0 M, *m*/*n* = 0.42/0.25 M), (**C**) Gelatin-KCl-$FeCN^{4-/3-}$ (*x* = 0.8 M, *m*/*n* = 0.42/0.25 M). The hysteresis loop was scanned at the speed of 180 s/cycle. Time dependent voltage difference $\Delta V = V(T_C) - V(T_H)$ and temperature difference $\Delta T = T_H - T_C$ for: (**D**) Gelatin-KCl, (**E**) Gelatin-$FeCN^{4-/3-}$, (**F**) Gelatin-KCl-$FeCN^{4-/3-}$. The direction of temperature gradient was reversed during the cycling test. The hysteresis loop displayed the different shapes, i.e. a slimly bar-like shape (Gelatin-KCl) (A), an egg-like shape (Gelatin-$FeCN^{4-/3-}$) (B) and a rhomboid shape (Gelatin-KCl-$FeCN^{4-/3-}$) (C).

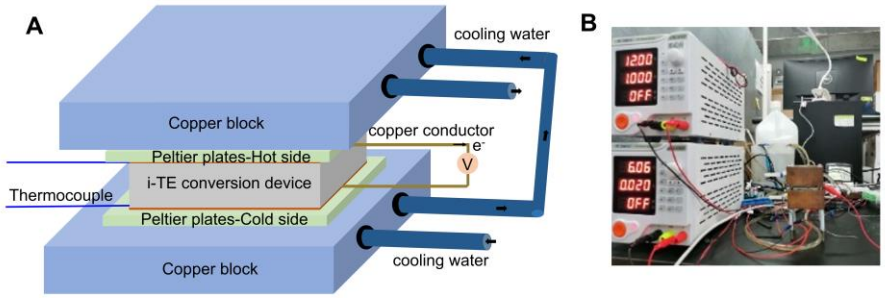

Fig. S13. (**A**) Schematic and (**B**) real picture of measurement setup for i-TE conversion.

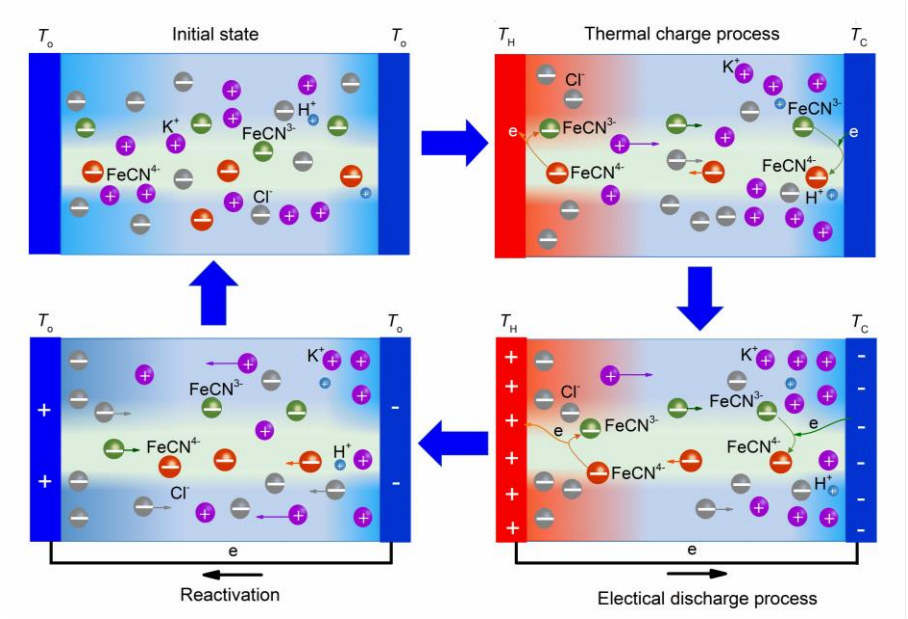

Fig. S14. Operation cycle of the i-TE cell: initial state, thermal charge process, electrical discharge process and reactivation.

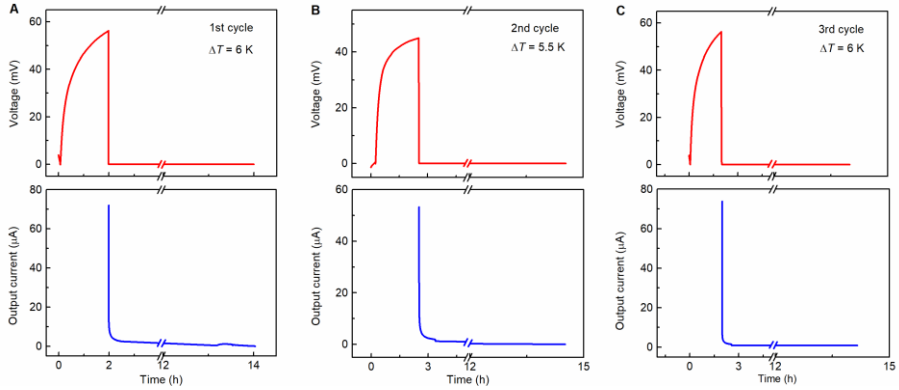

Fig. S15. Open-circuit voltage and close-circuit output current of i-TE cell (Cu | Au | i-TE | Au | Cu, 15 × 15 × 1.8 mm, Au (40 nm) coated rough Cu foils; i-TE: Gelatin-0.8M KCl-0.42/0.25M $FeCN^{4-/3-}$ (r_v = 2.0)) for (**A**) the 1st cycle, (**B**) the 2nd cycle (**C**) the 3rd cycle, which the cooling down was operated before each thermal charge process. The thermally charged voltage was ~2 h, and then the close-circuit discharge continued for 12 h at the constant temperature difference. The voltage in the close-circuit discharge was normalized to zero. After the electrical discharge, the i-TE cell was cooled down and close-circuited to reactivate. The i-TE cell was encapsulated by medical Vaseline and then a polyethylene film.

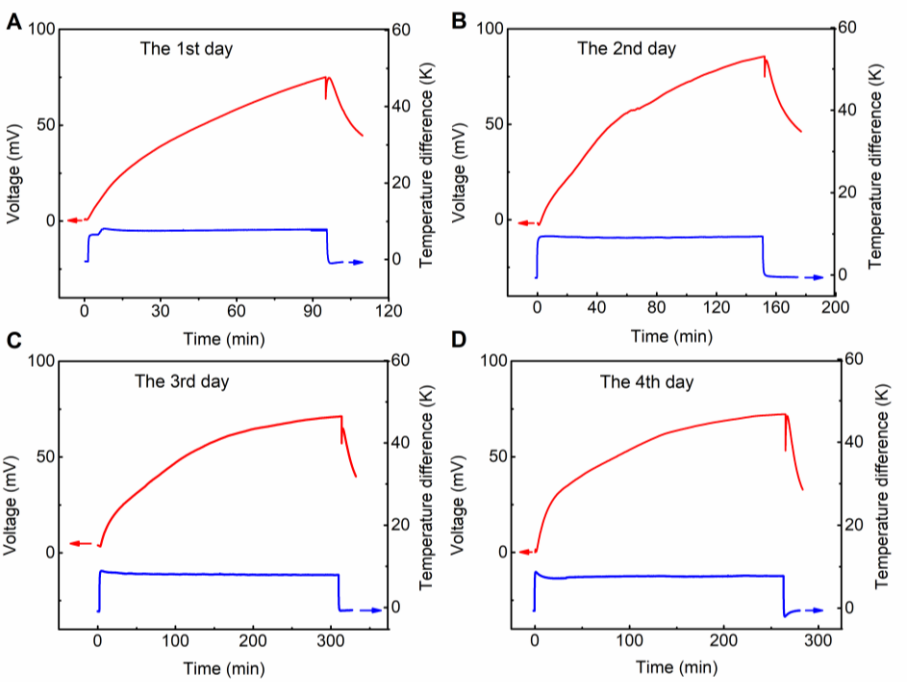

Fig. S16. The thermally charged voltage at different measuring days for the i-TE cell (Cu | Au | i-TE | Au | Cu, 15 × 15 × 1.8 mm, Au (40 nm) coated rough Cu foils; i-TE: Gelatin-0.8M KCl-0.42/0.25M $FeCN^{4-/3-}$ (r_v = 2.0)), (**A**) the 1st day, (**B**) the 2nd day, (**C**) the 3rd day, (**D**) the 4th day. The cell was encapsulated by medical Vaseline and then a polyethylene film for suppressing the water evaporation. After the measurement, two electrodes of i-TE cell were directly connected.

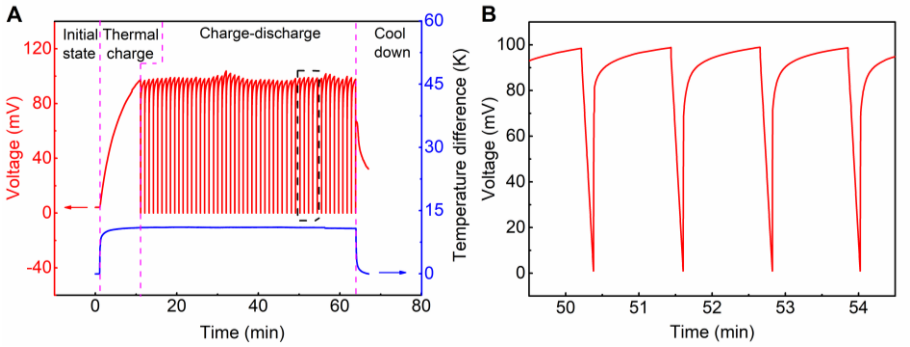

Fig. R17. (**A**) Quasi-continuous thermal-charge/electrical-discharge process for a 3-layered i-TE cell of Gelatin-0.8M KCl-0.42/0.25M $FeCN^{4-/3-}$ (r_v = 2.0) (Cu | i-TE | Cu, 15 × 15 × 1.8 mm, Cu foil with smooth surface) for 50 cycles, (**B**) Enlarged image shown in the dashed box of Fig. A. The electrical discharge was conducted in a direct close-circuit.

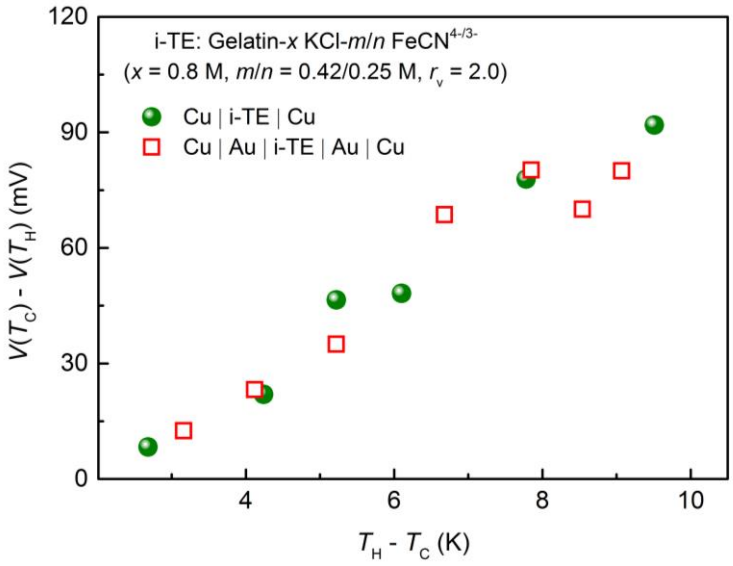

Fig. S18. Thermopower measurement for the as-fabricated i-TE cells Cu | i-TE | Cu and Cu | Au | i-TE | Au | Cu, where i-TE represented Gelatin-0.8M KCl-0.42/0.25M $FeCN^{4-/3-}$ (r_v = 2.0). Au (40 nm) was coated on the Cu foil with smooth surface by ion sputtering.

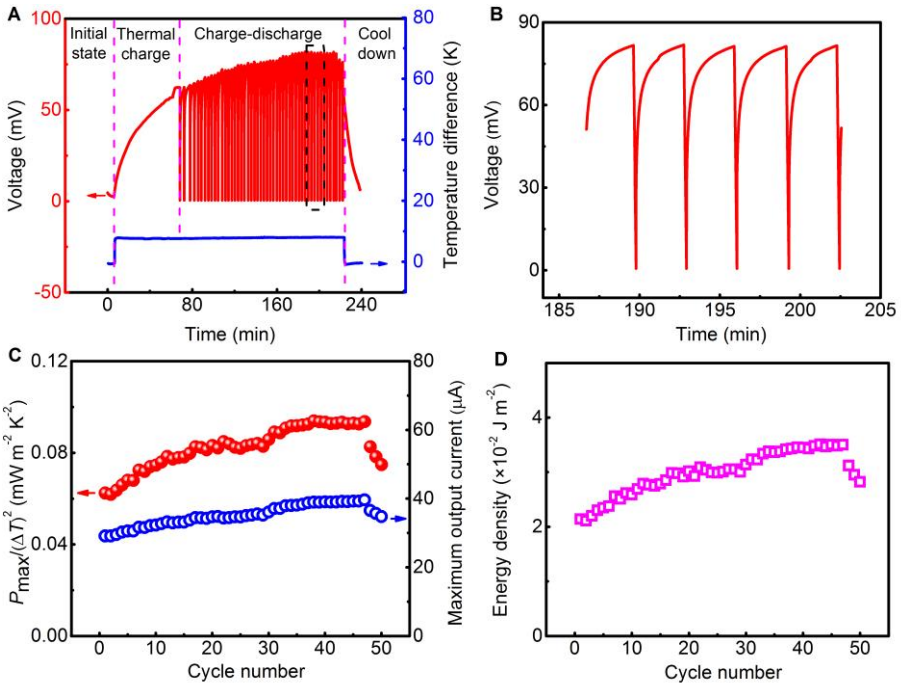

Fig. S19. (**A**) Quasi-continuous thermal-charge/electrical-discharge process for an i-TE cell of Gelatin-0.8M KCl-0.42/0.25M $FeCN^{4-/3-}$ (r_v = 2.0) (Cu | i-TE | Cu, 15 × 15 × 1.8 mm, Cu foil with smooth surface) for 50 cycles at ΔT = 7.5 K. (**B**) Enlarged image shown in the dash box of Fig. A. (**C**) Corresponding $P_{max}/(\Delta T)^2$ and maximum output current varying with the cycle number. (**D**) Corresponding energy density varying with the cycle number. The energy was calculated by integrating the output power with respect to time.

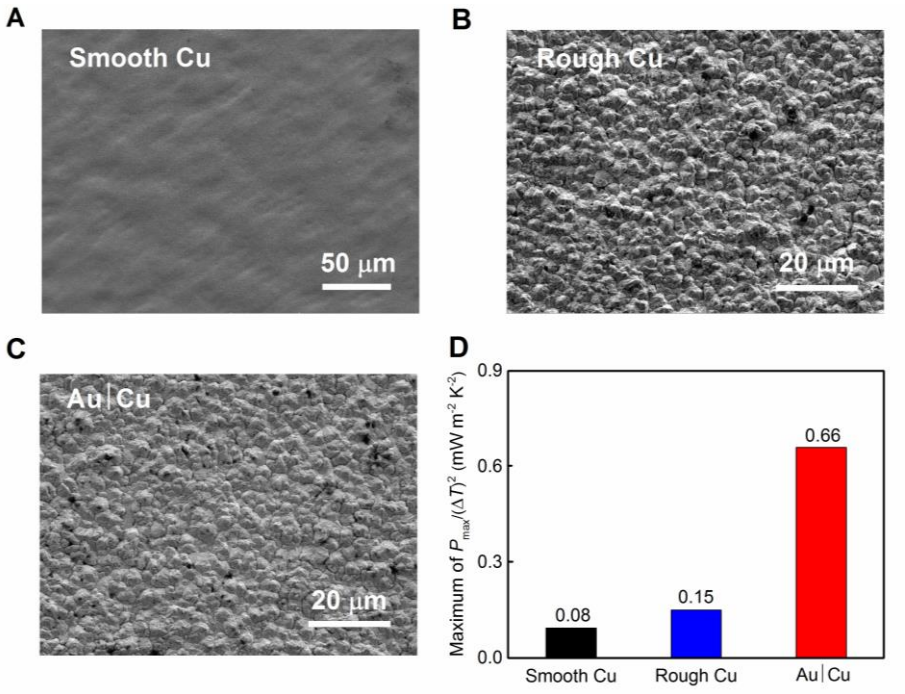

Fig. S20. SEM of (**A**) Cu foil with smooth surface, (**B**) Cu foil and (**C**) Au (40 nm)-coated Cu foil with rough surface. (**D**) Maximum of $P_{max}/(\Delta T)^2$ for i-TE cell (15 × 15 × 1.8 mm, i-TE: Gelatin-0.8M KCl-0.42/0.25M $FeCN^{4-/3-}$ (r_v = 2.0)) in a quasi-continuous thermal charge/electrical discharge work mode. The rough surface Cu foil electrode in an i-TE cell operated for 30 cycles at ΔT = 11 K. As compared with the i-TE cell with smooth surface Cu foil, the one with Au coated Cu foil has 2-3 times improved output current due to the increased surface area, and hence significantly increases $P_{max}/(\Delta T)^2$. Alzahrani *et al* reported a similarly enhanced output current in the ferri/ferrocyanide thermogalvanic cells by using Au-nanoparticles immobilised at the gel/electrode interface (44).

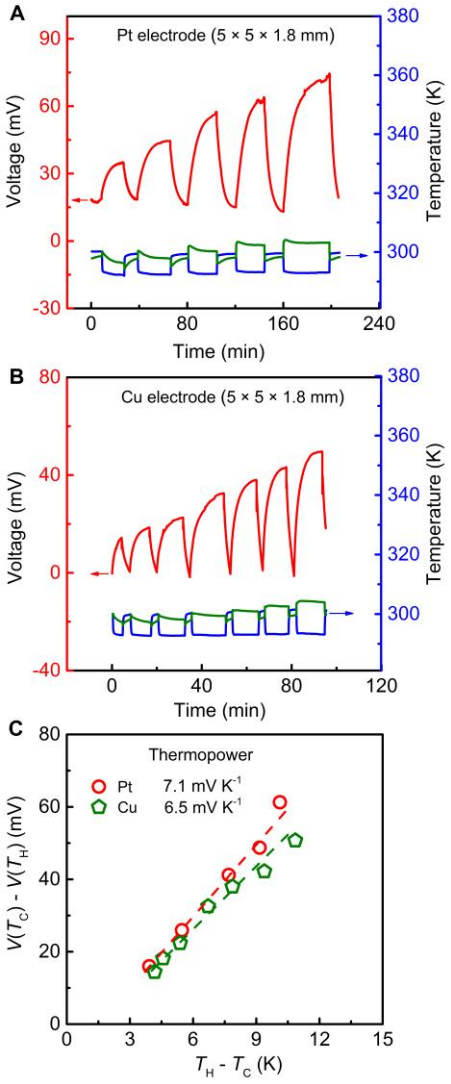

Fig. S21. Effect of electrode on the thermopower. Thermopower measurement of i-TE material of Gelatin- 0.8M KCl with (**A**) Pt electrode (Pt | i-TE | Pt, 5 × 5 × 1.8 mm) and (**B**) Cu foil electrode (Cu | i-TE | Cu, 5 × 5 × 1.8 mm). (**C**) Thermopower measurement of the i-TE material (Gelatin- 0.8M KCl) with different electrodes, showing the 7.1 and 6.5 mV K^{-1} for the Pt electrode and Cu electrode, respectively. It suggests that the thermopower is relatively independent of the choice of electrode. The $V(T_C) - V(T_H)$ is the voltage difference, while the $T_H - T_C$ is the temperature difference.

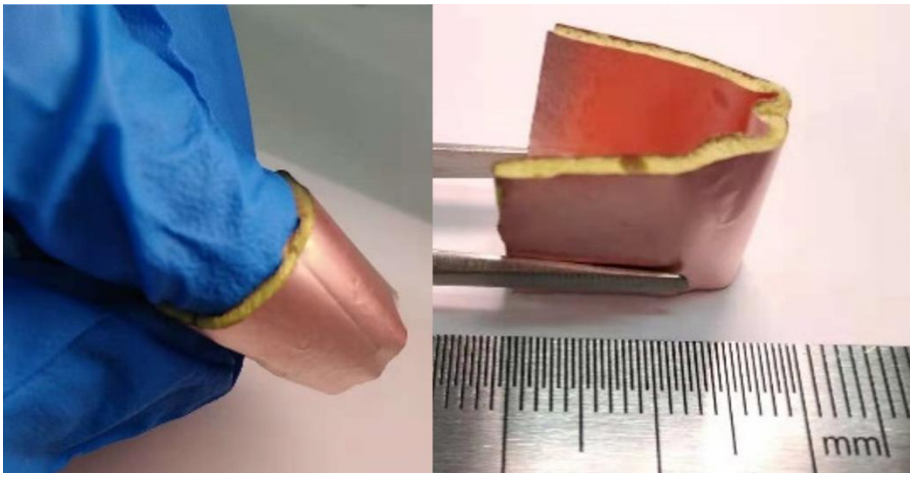

Fig. S22. Images of the as-fabricated flexible i-TE single cell made by the Gelatin-0.8M KCl-0.42/0.25M $FeCN^{4-}$ /$^{3-}$(, r_v = 2.0).

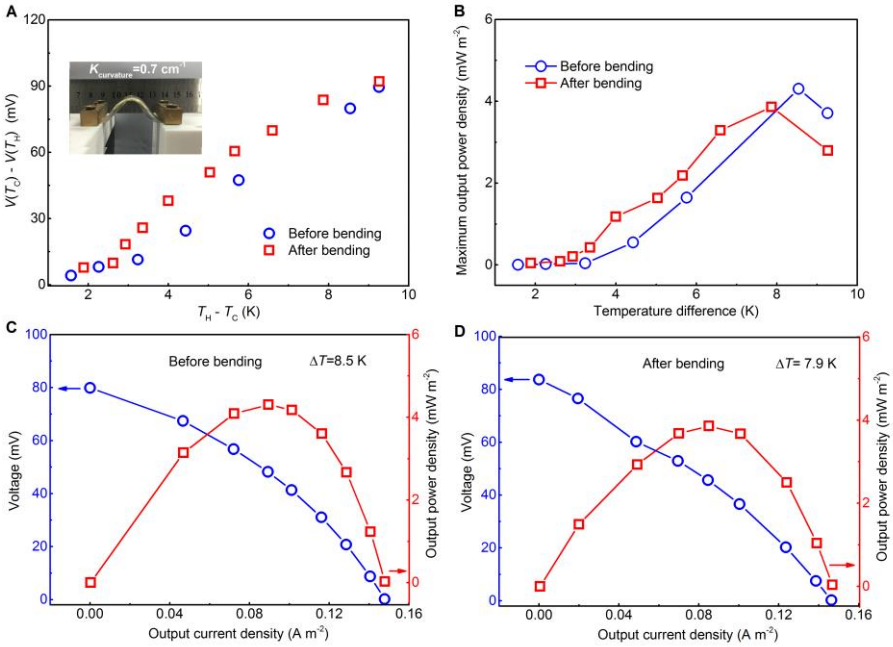

Fig. S23. (**A**) Thermopower measurement of the i-TE materials of Gelatin-0.8M KCl-0.42/0.25M $FeCN^{4-/3-}$(, r_v = 2.0, Cu foil with smooth surface) before and after 5000 cycles bending. The $V(T_C) - V(T_H)$ is the voltage difference, while the $T_H - T_C$ is the temperature difference. The inset showed the picture of the bending experiment with the curvature of 0.7 cm^{-1}. (**B**) The corresponding maximum output power density versus temperature difference. Voltage-current-output power curves of i-TE single cell (Cu | i-TE | Cu) (**C**) before bending and (**D**) after 5000 cycles bending. The bending has negligible effect on the performance, with normalized maximum power density $P_{output,max}/\Delta T^2$ even slightly from 0.060 mW m^{-2} K^{-2} (C) to 0.062 mW m^{-2} K^{-2} (D).

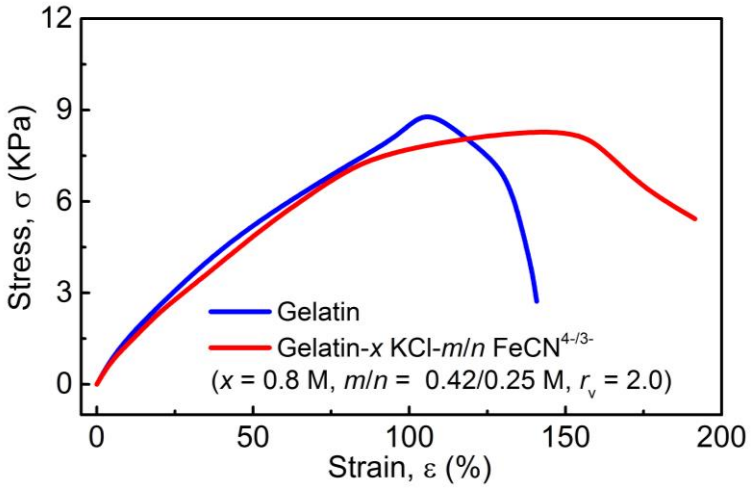

Fig. S24. (**A**) Strain versus stress curves of the i-TE material of Gelatin-0.8M KCl-0.42/0.25M $FeCN^{4-/3-}$ (r_v = 2.0), compared with the pure Gelatin. The better behavior of the i-TE material of Gelatin-0.8M KCl-0.42/0.25M $FeCN^{4-/3-}$ (r_v = 2.0) could be resulted from the interaction between the gelatin network and K^+, Cl^- and $FeCN^{4-/3-}$.

Table S1. Comparison of the thermopower and references for Figure 1B in the main text.

Label name	Thermopower (mV K^{-1})	Reference
Li	+24	30
Bonetti	+7	51
Zhao	+14	29
Duan*	+4.2	22
Kim*	+2.9	20
Buckingham#	-1.46	13
Kang*	+1.4	16
Duan##	-1.9	45
Jin###	+1.4	54
Wu####	+1.1	55

*: $FeCN^{4-/3-}$ aqueous electrolyte.

#: Fe(II)/Fe(III) aqueous electrolyte.

##: N-isopropylacrylamide based I^-/I^{3-} nanogels.

###: Cellulose based $FeCN^{4-/3-}$ nanogels.

####: Poly(sodium acrylate) based $FeCN^{4-/3-}$ gels.

$FeCN^{4-/3-}$ represents the $Fe(CN)_6^{4-}/Fe(CN)_6^{3-}$ in $K_4Fe(CN)_6/K_3Fe(CN)_6$.

Table S2. Comparison of the $P_{max}/(\Delta T)^2$ for the quasi-solid state based i-TE materials.

Redox couple	Matrix	$P_{max}/(\Delta T)^2$ (mW K^{-2} m^{-2})	Reference
$FeCN^{4-/3-}$	Gelatin	0.66	This work
$FeCN^{4-/3-}$	Cellulose	0.06	54
$FeCN^{4-/3-}$	Poly(sodium acrylate)	0.003	55
$FeCN^{4-/3-}$	Poly(vinyl alcohol) (PVA)	0.02	28
I^-/I^{3-}	N-isopropylacrylamide	0.07	45
$[Co(bpy)_3]^{2+/3+}[NTf_2^-]_{2/3}$	Poly(vinylidene fluoride-co-hexafluoropropene) (PVDF-HFP)	0.001	56
$[Co(bpy)_3]^{2+/3+}[NTf_2^-]_{2/3}$	Polyvinylidene difluoride and 3-methoxypropionitrile (PVDF-MPN)	0.009	57

References

1. J. He, T. M. Tritt, Advances in thermoelectric materials research: Looking back and moving forward. *Science* **357**, 1369 (2017).

2. M. Haras, T. Skotnicki, Thermoelectricity for IoT–A review. *Nano Energy* **54**, 461-476 (2018).

3. E. Mu et al., A novel self-powering ultrathin TEG device based on micro/nano emitter for radiative cooling. *Nano Energy* **55**, 494-500 (2019).

4. B. Iezzi, K. Ankireddy, J. Twiddy, M. D. Losego, J. S. Jur, Printed, metallic thermoelectric generators integrated with pipe insulation for powering wireless sensors. *Appl. Energy* **208**, 758-765 (2017).

5. R. Zito, Thermogalvanic energy conversion. *AIAA J.* **1**, 2133-2138 (1963).

6. T. I. Quickenden, Y. Mua, A review of power generation in aqueous thermogalvanic cells. *J. Electrochem. Soc.* **142**, 3985-3994 (1995).

7. E. D. Eastman, Theory of the Soret effect. *J. Am. Chem. Soc*. **50**, 283-291 (1928).

8. H. J. V. Tyrrell, D. A. Taylor, C. M. Williams, The 'Seebeck effect' in a purely ionic system, *Nature* **177**, 668-669 (1956).

9. R. Hu et al., Harvesting waste thermal energy using a carbon-nanotube-based thermoelectrochemical cell. *Nano Lett.* **10**, 838-846 (2010).

10. D. Zhao et al., Ionic thermoelectric supercapacitors. *Energy Environ. Sci.* **9**, 1450-1457 (2016).

11. T. J. Abraham, D. R. MacFarlane, J. M. Pringle, High Seebeck coefficient redox ionic liquid electrolytes for thermal energy harvesting. *Energy Environ. Sci.* ***6***, 2639-2645 (2013).

12. M. A. Lazar, D. Al-Masri, D. R. MacFarlane, J. M. Pringle, Enhanced thermal energy harvesting performance of a cobalt redox couple in ionic liquid–solvent mixtures. *Phys. Chem. Chem. Phys.* **18**, 1404-1410 (2016).

13. M. A. Buckingham, F. Marken, L. Aldous, The thermoelectrochemistry of the aqueous iron(ii)/iron(iii) redox couple: significance of the anion and pH in thermogalvanic thermal-to-electrical energy conversion. *Sustain. Energy Fuels* **2**, 2717-2726 (2018).

14. T. J. Abraham, D. R. MacFarlane, J. M. Pringle, Seebeck coefficients in ionic liquids–prospects for thermo-electrochemical cells. *Chem. Commun.* **47**, 6260-6262 (2011).

15. T. J. Abraham et al., Towards ionic liquid-based thermoelectrochemical cells for theharvesting of thermal energy. *Electrochim. Acta* **113**, 87-93 (2013).

16. T. J. Kang et al., Electrical power from nanotube and graphene electrochemical thermal energy harvesters. *Adv. Funct. Mater.* **22**, 477-489 (2012).

17. M. S. Romano et al., Carbon nanotube–reduced graphene oxide composites for thermal energy harvesting applications. *Adv. Mater.* **25**, 6602-6606 (2013).

18. Y. Yang et al., Charging-free electrochemical system for harvesting low-grade thermal energy. *Proc. Natl. Acad. Sci. U.S.A.* **111**, 17011-17016 (2014).

19. H. Im et al., High-efficiency electrochemical thermal energy harvester using carbon nanotube aerogel sheet electrodes. *Nat. Commun.* **7**, 10600 (2016).

20. T. Kim et al., High thermopower of ferri/ferrocyanide redox couple in organic-water solutions. *Nano Energy* **31**, 160-167 (2017).

21. L. Zhang et al., High power density electrochemical thermocells for inexpensively harvesting low-grade thermal energy. *Adv. Mater.* **29**, 1605652 (2017).

22. J. Duan et al., Aqueous thermogalvanic cells with a high Seebeck coefficient for low-grade heat harvest. *Nat. Commun.* **9**, 5146 (2018).

23. J. H. Kim et al., Iron (II/III) perchlorate electrolytes for electrochemically harvesting low-grade thermal energy. *Sci. Rep.* 9, 8706 (2019).

24. Y. V. Kuzminskii, V. A. Zasukha, G. Y. Kuzminskaya, Thermoelectric effects in electrochemical systems. Nonconventional thermogalvanic cells. *J. Power Sources* **52**, 231-242 (1994).

25. S. L. Kim, H. T. Lin, C. Yu, Thermally chargeable solid-state supercapacitor. *Adv. Energy Mater.* **6**, 1600546 (2016).

26. H. Ma et al., Powerful thermogalvanic cells based on a reversible hydrogen electrode and gas containing electrolytes. *ACS Energy Lett.* 4, 1810-1815 (2019).

27. A. Kundu, T. S. Fisher, Harnessing the thermogalvanic effect of the ferro/ferricyanide redox couple in a thermally chargeable supercapacitor. *Electrochim. Acta* **281**, 357-369 (2018).

28. P. Yang et al., Wearable thermocells based on gel electrolytes for the utilization of body heat. *Angew. Chem. Int. Edit.* **55**, 12050-12053 (2016).

29. D. Zhao et al., Polymer gels with tunable ionic Seebeck coefficient for ultra-sensitive printed thermopiles. *Nat. Commun.* **10**, 1093 (2019).

30. T. Li et al., Cellulose ionic conductors with high differential thermal voltage for low-grade heat harvesting. *Nat. Mater.* **18**, 608-613 (2019).

31. A. J. deBethune, T. S. Licht, N. Swendeman, The temperature coefficients of electrode potentials. *J. Electrochem. Soc*. **106**, 616-625 (1959).

32. S. C. Bratsch, Standard electrode potentials and temperature coefficients in water at 298.15 K. *J. Phys. Chem. Ref. Data* **18**, 1-21 (1989).

33. Materials and Methods are available as Supplementary Materials on Science Online

34. J. N. Agar, C. Y. Mou, J. L. Lin, Single-ion heat of transport in electrolyte solutions: a hydrodynamic theory. *J. Phys. Chem*. **93**, 2079-2082 (1989).

35. B. Huang et al., Non-covalent interactions in electrochemical reactions and implications in clean energy applications. *Phys. Chem. Chem. Phys*. **20**, 15680-15686 (2018).

36. C. M. Ofner III, H. Schott, Shifts in the apparent ionization constant of the carboxylic acid groups of gelatin. *J. Pharm. Sci.***74**, 1317-1321 (1985).

37. S. Duhr, D. Braun, Why molecules move along a temperature gradient. *Proc. Natl. Acad. Sci. U.S.A*. **103**, 19678-19682 (2006).

38. J. Kamcev, D. R. Paul, G. S. Manning, B. D. Freeman, Ion diffusion coefficients in ion exchange membranes: Significance of counterion condensation. *Marcromolecules* **51**, 5519-5529 (2018).

39. D. Aryal, V. Ganesan, Reversal of salt concentration dependencies of salt and water diffusivities in polymer electrolyte membranes. *ACS Marcro Lett*. **7**, 739-744 (2018).

40. D. Aryal, V. Ganesan, Impact of cross-linking of polymers on transport of salt and water in polyelectrolyte membranes: A mesoscopic simulation study. *J. Chem. Phys.* **149**, 224902 (2018).

41. G. S. Mannining, Limiting laws and counterion condensation in polyelectrolyte solutions. 8. mixtures of counterions, species selectivity, and valence selectivity. *J. Phys. Chem.* **88**, 6654-6661 (1984).

42. D. J. Tobias, J. C. Hemminger, Getting specific about specific ion effects. *Science* **319**, 1197 (2008).

43. A. Al-zubaidi, X. Ji, J. Yu, Thermal charging of supercapacitors: a perspective. *Sustain. Energy Fuels* **1**, 1457-1474 (2017).

44. H. A. H. Alzahrania, M. A. Buckingham, F. Marken, L. Aldous, Success and failure in the incorporation of gold nanoparticles inside ferri/ferrocyanide thermogalvanic cells. *Electrochem. Commun*. **102**, 41-45 (2019).

45. J. Duan et al., P-N conversion in thermogalvanic cells induced by thermo-sensitive nanogels for body heat harvesting. *Nano Energy* **57**, 473-479 (2019).

46. S. J. Kim, J. H. We, B. J. Cho, A wearable thermoelectric generator fabricated on a glass fabric. *Energy Environ. Sci.* **7**, 1959-1965 (2014).

47. J. Y. Oh et al., Chemically exfoliated transition metal dichalcogenide nanosheet-based wearable thermoelectric generators. *Energy Environ. Sci.* **9**, 1696-1705 (2016).

48. C. S. Kim et al., Structural design of a flexible thermoelectric power generator for wearable applications. *Appl. Energy* **214**, 131-138 (2018).

49. G. Chen, *Nanoscale Energy Transport and Conversion*, *Oxford Press*, (2005).

50. P. K. Pathria, P. D. Beale, *Statistical Mechanics*, *Academic Press*, (2011).

51. M. Bonetti, S. Nakamae, M. Roger, P. Guenoun, Huge Seebeck coefficients in nonaqueous electrolytes. *J. Chem. Phys*. **134**, 114513 (2011).

52. Y. Marcus, Effect of ions on the structure of water: Structure making and breaking. *Chem. Rev*. **109**, 1346-1370 (2009).

53. A. J. Bard, L. R. Faulkner, *Electrochemical Methods: Fundamentals and Applications*, 2nd Edition, New York: Wiley, (2008).

54. L. Jin, G. W. Greene, MacFarlane, D. R. MacFarlane, J. M. Pringle, Redox-active quasi-solid-state electrolytes for thermal energy harvesting. *ACS Energy Lett*. **1**, 654-658 (2016).

55. J. Wu, J. J. Black, L. Aldous, Thermoelectrochemistry using conventional and novel gelled electrolytes in heat-to-current thermocells. *Electrochim. Acta* **225**, 482-492 (2017).

56. A. Taheri, D. R. MacFarlane, C. Pozo-Gonzalo, J. M. Pringle, Flexible and non-volatile redox active quasi-solid state ionic liquid based electrolytes for thermal energy harvesting. *Sustainable Energy Fuels* **2**, 1806-1812 (2018).

57. A. Taheri, D. R. MacFarlane, C. Pozo-Gonzalo, J. M. Pringle, Quasi-solid-state electrolytes for low-grade thermal energy harvesting using a cobalt redox couple. *ChemSusChem* **11**, 2788-2796 (2018).